# APPENDIX A

P-54

## AC IMPEDANCE ANALYSIS OF POLYPYRROLE THIN FILM

# AC Impedance Analysis of Polypyrrole Thin Films

Reginald M. Penner** and Charles R. Martin*

*Department of Chemistry*

*Texas A&M University*

*Electrochemical Society Active Member, to whom correspondence should be addressed.

**Electrochemical Society Student Member, Present Address:

Department of Chemistry, Stanford University

Stanford, CA 94305

ABSTRACT

The AC impedance spectra of thin (0.27 $\mu$m) polypyrrole films have been obtained at open circuit potentials from -0.4 V to 0.4 V vs. SCE. Two limiting cases are discussed for which simplified equivalent circuits are applicable. At very positive potentials, the predominently nonfaradaic AC impedance of polypyrrole is very similar to that observed previously for finite porous metallic films. Modeling of these data with the appropriate equivalent circuit permits effective pore diameter and pore number densities of the oxidized film to be estimated.

At potentials from -0.4 V to -0.3 V, the polypyrrole film is essentially nonelectronically conductive and diffusion of polymer oxidized sites with their associated counterions can be assumed to be linear from the film/substrate electrode interface. The equivalent circuit for the polypyrrole film at these potentials is that previously described for metal oxide, lithium intercalation thin films. Using this model, counterion diffusion coefficents are determined for both semi-infinite and finite diffusion domains. The diffusion coefficient data so obtained is consistant with the existance of a gradient in the morphology of the polypyrrole films in a direction normal to the surface of the electrode.

In addition, the limiting low frequency resistance and capacitance of the polypyrrole thin films is determined and compared to that obtained previously for thicker films of the polymer. The origin of the observed potential dependence of these low frequency circuit components is discussed.

## INTRODUCTION

A number of technological applications for electronically conductive polyheterocycles (eg. polypyrrole, polythiophene) have been demonstrated in recent years. These include the application of polyheterocyclic films as potentiostatically controlled ion-gates (1,2), in electrochromic displays (cf.3,4), as battery cathode materials (5-8), and in chemically responsive transistors (9-11). All of these applications rely on the ability of the electronically conductive polymer to "switch" rapidly and reversibly between insulating and conducting redox states. The rate of the polymer redox reaction for electrochemically synthesized conducting polymers has been shown to be inversely related to the thickness of the polymer film (8,10,12) For this reason, the design of polymer-based devices has emphasized the use of extremely thin ($l < 1$ $\mu$m) polymer films (8,10,12).

Despite the importance of polyheterocyclic films of submicron thickness, little is currently known about mass transport in these thin films. Previous AC impedance studies of polypyrrole by Burgemayer and Murray (1,2) and more recently by Tanguy et al. (13,14) have employed relatively thick ($> 5$ $\mu$m) polymer films. Such films cannot be quantitatively addressed electrochemically; ie., as-synthesized oxidized polymer cannot be quantitatively reduced (15,16). Consequently, the extraction of mass transport and kinetic information from this data is not straightforward. Bull et al. examined the AC impedance behavior of thin polypyrrole films over a broad frequency band but did not consider mass transport in the analysis of these data (17). Glarum et al. has recently published an analysis of the potential dependant AC impedance behavior of thin electronically conductive polyaniline films (18).

Recently, AC impedance analyses have been applied to the determination of diffusion coefficients in electrochromic $WO_3$ films (19) and in redox polymer film modified electrodes (20). This work has demonstrated that transport information can be obtained from AC impedance data for any system which exhibits finite, linear diffusion, providing the heterogeneous electron transfer kinetics of the system are suitably fast. AC impedance possesses several advantages for the determination of diffusion coefficients as compared to conventional, large amplitude, electrochemical experiments such as chronocoulometry. In contrast to Cottrell-type experiments in which diffusion coefficient information is obtained while the system is in flux from one redox state to another, the perturbation of the film redox state during an AC impedance experiment is extremely small permitting transport information to be obtained for any discrete ratio [Ox]/[Red]. Consequently, morphological changes in the film structure which can accompany a bulk conversion from one redox state to another are avoided; characteristics of the film associated with a particular redox state can be elucidated. In addition, a wide band of frequencies can be addressed in an AC impedance experiment allowing the characteristic time-scale of an electrochemical process, such as diffusion, to be isolated as the corresponding frequency interval and differentiated from events with other characteristic time-scales. Consequently, both kinetic and mass transport information can obtained from the same experiment.

In this paper, we interpret the AC impedance data obtained for 0.27 $\mu$m $\pm$ 0.02 $\mu$m films in the context of the limiting behavior which is observed for polypyrrole films at low doping levels and for fully oxidized films. In the former case (Limiting Case I), the polymer film is essentially

nonelectronically conductive. The equivalent circuit appropriate for this system is that described by of Ho et al. (19) and by Franceschetti et al. (21-23). As noted above, diffusion coefficient information has been obtained using this technique for a number of functionally similar systems including $WO_3$ lithium intercalation films (19,21-23) and Nafion polymer modified electrodes (20,24).

The AC impedance of oxidized polypyrrole (Limiting Case II) has previously been described in terms of a porous electrode model by Bull et al. (16) and by Burgmayer et al. (1,2). However, a more rigorous model has recently been demonstrated for finite, porous electrodes by Keiser et al. (25) and by Candy et al. (26). The latter model permits film parameters such as the equivalent cylindrical pore diameter and pore number density to be calculated from the AC impedance spectra of finite porous films (26). In the present case, the AC impedance observed for oxidized polypyrrole films is interpretted using the analysis of Candy and coworkers (26).

In addition, the limiting low frequency resistance and capacitance of the polypyrrole thin films is determined and compared to that obtained previously for thicker films of the polymer (13,14). The origin of the observed potential dependence of these low frequency circuit components is discussed.

## THEORY

*Limiting Case I: Lightly Doped Polymer.*

As noted above, a number of recent papers describe the interpretation of AC impedance data for transition metal intercalation compounds (19, 21-23) and redox polymer modified electrodes (20,24). In both of these

systems, a redox couple is confined to a thin film, and the diffusion of the electroactive species in each is finite and linear. We have chosen to use the analysis of Ho et al. because it explicitly treats the limiting cases applicable to polypyrrole (19). The authors have made a number of assumptions in the derivation of this model which need to examined here in the context of the application of this theory to electronically conductive polymers. Two of these assumptions are particularly important: 1) diffusion of the intercalating species is linear, and 2) the Warburg impedance is that due to the diffusion of a single species ($Li^o$) and hence can be characterized by a single diffusion coefficient (19).

In the case of $Li_yWO_3$ and other electronically conductive transition metal oxide films, it is commonly assumed that intercalation of $Li^+$ is preceded by charge transfer and ion pair formation, $Li_y^+WO_3^-$ (or $Li_yWO_3$), at the oxide film/electrolyte interface (19,22). Because intercalation of the $Li^+$ is commensurate with charge transfer, $Li^o$ is the only mobile species in the film. Diffusion of the intercalated $Li^o$ then occurs linearly from the film/electrolyte interface. A key point regarding the applicability of the data analysis technique employed by Ho et al. to polyheterocyclic films is the extent to which diffusion in the conducting polymer film is linear. At potentials where polypyrrole is a good electronic conductor ($E_{oc}$ > 0.3 V vs. SCE), diffusion cannot be assumed to be linear since the polymer redox reaction can proceed from any conductive surface in the porous film. However, at open circuit potentials from -0.4 V to -0.3 V (100-200 mV negative of $E^{o\prime}$), where the polypyrrole is lightly doped, the data from the present paper as well as previous experimental evidence (27,28) indicates that the conductivity of the polymer is very low. As the bulk electronic

conductivity of the polymer is low, the redox reaction of the polymer can be assumed to proceed only from the Pt substrate/polymer interface. Hence, it is assumed here that diffusion of oxidized polymer sites (and charge compensating anions) is linear from the Pt substrate/polymer interface at potentials < 0.3 V vs. SCE.

The diffusion coefficient for the diffusion of intercalated $Li^{o}$ in a metal oxide matrix is many orders of magnitude smaller than that for the diffusion of $Li^{+}$ in the contacting electrolyte (ca. $10^{-12}$ vs. $10^{-5}$ $cm^2$ $sec^{-1}$ (19)). In contrast to AC impedance analyses of redox couples in solution (29), the diffusion limited current for $Li_yWO_3$ is always dictated by slow diffusion of $Li^{o}$ and the expression for the Warburg impedance incorporates a single diffusion coefficient (19,23). It is less clear in the case of polypyrrole if the Warburg impedance can be assumed to be dominated by a single diffusing species, eg. diffusion of the anion. The polymer redox reaction for polypyrrole can be written:

$$PPy^{o} + A^{-} \text{-----} > PPy^{+}A^{-} + e^{-}$$

Diffusion of $PPy^{+}$ sites generated by an AC varying potential signal might be limited by the diffusion of the anion, $A^{-}$, diffusion of the counterion, $C^{+}$, electron diffusion; (i.e., the rate of electron hopping), or some combination of these. Buttry and coworkers have performed quartz crystal microbalance (QCM) gravimetry on thin polypyrrole and polythiophene films synthesized in acetonitrile (30). These data indicate that bulky tetrabutylammonium cations are excluded from polypyrrole films during oxidation-reduction cycles (30). Under these circumstances, if electron

hopping can be assumed to be facile, diffusion of $PPy^+$ will be limited by codiffusion of charge compensating $BF_4^-$ anions. Again, a single diffusion coefficient, $D_{BF4-}$, is adequate to describe the diffusion limited current. The application of the data analysis technique of Ho et al. to nonpermselective polypyrrole films will yield diffusion coefficients which are composite values containing contributions from both anion and cation diffusion (20,29).

AC impedance analysis of polypyrrole, then, can be made to conform to the assumptions made by Ho et al. by insuring that the polymer is not electronically conductive at the potentials at which diffusion coefficient information is obtained, and by employing a tetrabutylammonium cation which is excluded from the polymer film.

The model proposed by Ho et al. assumes the Randles equivalent circuit shown in Figure 1A (31). However, the usual form of the Warburg (diffusional) impedance is modified to compensate for the finite diffusion length of ions in a thin film. The detailed derivation of these expressions is found in reference 19. The explicit form of the finite Warburg impedance is (19):

$$Z_w = R_w - jX_w \tag{1}$$

where:

$$Xw = (\omega C_w)^{-1} = |Z_w| \sin \beta \tag{2}$$

$$Rw = |Z_w| \cos \beta \tag{3}$$

$$|Zw| = |\nu_o / i_o a| \tag{4}$$

where $\nu_o$ is the AC potential amplitude, a is the electrode area, and $C_w$ and

Rw are the Warburg capacitance and resistance respectively. The Warburg phase angle, $\beta$, is defined as:

$$\beta = \arctan \frac{(\sinh(2kl))+(\sin(2kl))}{(\sinh(2kl))-(\sin(2kl))} \tag{5}$$

with:

$$k = (\omega/2D)^{1/2} \tag{6}$$

where $\omega$ is the angular frequency of the applied AC signal and D is the diffusion coefficient of the counterion, $BF_4^-$. The current amplitude, $i_o$, is defined as:

$$io = -\frac{zF}{2}\frac{dC_{BF4-}}{dE}\nu_o\,(\omega D)^{1/2}\left(\frac{h2 + s2}{d2}\right)^{1/2} \tag{7}$$

where $dC_{BF4-}/dE$ is the gradient of polymer oxidation state, and hence $BF_4^-$ concentration, with open circuit potential. The expressions for the equivalent series resistance, $R_s$, and capacitance, $C_s$, elements of the faradaic impedance (incorporating the finite Warburg elements (Eq. 2,3)) are given by (29):

$$R_s = R_{ct} + R_w = R_{ct} + |\nu_o/i_o a| \cos\beta \tag{8}$$

$$C_s = C_w = (|\nu_o\omega/i_o a| \sin\beta)^{-1} \tag{9}$$

where $R_{ct}$ is the charge transfer resistance; $R_{ct} = RT/zFI_o$. The expressions for the real, Z[re], and imaginary, Z[im], components of the total impedance are obtained by substituting Eq. 8 and Eq. 9 into the expressions for Z[re] and Z[im] in the Randles circuit (29,30):

$$Z[re] = R_u + \frac{R_s}{((C_d/C_s)+1)^2 + (\omega R_s C_d)^2} \tag{10}$$

$$Z[im] = \frac{\omega R_s^2 C_d + C_d/(C_s^2 \omega^1) + (\omega C_s)^{-1}}{((C_d/C_s)+1)^2 + (\omega R_s C_d)^2} \tag{11}$$

Where $R_u$ is the series resistance of the solution and the polymer film.

With these expressions, Nyquist diagrams can be generated for any combination of experimentally adjustable parameters. In practice, two important limiting subcases of Limiting Case I can be differentiated: IA) thick films and/or small diffusion coefficients ($kl \gg 1$), and, IB) thin films and/or large diffusion coefficients ($kl \ll 1$) (19).

Limiting Case IA corresponds to semi-infinite linear diffusion; ie., the maximum excursion of the diffusion layer at steady-state is less than the film thickness. In this case, $\beta$ becomes 45° and the Nyquist plot (Z[im] vs. Z[re]) is linear with a slope of 1. From this linear region, if dE/dC is known, the diffusion coefficient can be evaluated from the linear dependence of the impedance modulus, |Z|, with $\omega^{-1/2}$ (19):

$$|Z| = |[(dE)/(dC)][FD^{1/2}a]^{-1}w^{-1/2}| \tag{12}$$

In Limiting Case IB, the diffusion layer accesses the entire film volume corresponding to thin-layer electrochemical behavior. The Warburg phase angle, $\beta$, is $90^{o}$ and the Nyquist plot becomes vertical at a resistance of $(R_1+R_{ct}+R_u)$. The value of $R_1$, and hence the position of this vertical branch, is sensitive to the diffusion coefficient (19):

$$Z[re] = R_1 = \frac{1}{3nFaD}(dE/dC) \qquad (13)$$

The capacitance also becomes frequency independent under these conditions and equal to $C_1$ (19):

$$Z[im] = \frac{1}{\omega C_1} = |(dE/dC)/nF\omega la| \qquad (14)$$

Eqs. 13 and 14 may be used to calculate D and dC/dE simultaneously from $R_1$ and $C_1$ obtained from the low frequency region of the Nyquist plot.

For perfectly homogeneous films, the diffusion coefficients calculated from the semi-infinite frequency regime (Limiting Case IA) ought to agree with those obtained at frequencies corresponding to the finite diffusion case (Limiting Case IB).

*Limiting Case II: Oxidized Polymer.*

Although the theory for the AC impedance of porous electrodes is well established (32-34), only relatively recently has the AC impedance of thin, porous, metallic films been examined (25,26). The work of Kaiser et al. (25) and Candy et al. (26) has involved finite porous electrodes in contact

with electrolyte solutions containing no redox couple; systems for which the impedance is entirely nonfaradaic. Candy et al. have shown that porous metal layers in which the pores have irregular shapes (as, for example, in Raney-metal surfaces), exhibit impedance behavior similar to that predicted for surfaces consisting of cylindrically shaped pores of a uniform diameter (26). Such poorly defined metal films can be evaluated in terms of the pore radius, pore number density, and pore length of the equivalent cylindrical pore electrode (26).

Feldburg (35) and Burgemayer et al. (2) have calculated that the bulk capacitances of 100-200 C $cm^{-3}$ observed for oxidized polypyrrole films can only be accounted for if the specific capacitance of the polymer, and hence its conductivity, is very similar to that of metals. Oxidized polypyrrole films, then, might be expected to exhibit AC impedance behavior similar to that of porous metal layers. We have applied the recent model proposed by Candy et al. (26) to the analysis of the AC impedance observed for oxidized ($E_{oc}$ > +0.1 V vs. SCE) polypyrrole films in electrolyte solutions containing no electroactive species. The assumptions inherent in this analysis are simply that the conductivity of electrolyte in the pores of the electrode is known and is the same in all pores, and that the specific capacitance of the porous electrode surface, $C_{dl}$, is known and uniform. In addition, the capacitance of the Pt substrate electrode surface is assumed to be negligibly small relative to that of the porous bulk of the polymer.

The equivalent circuit for a single, electrolyte-filled cylindrical pore is shown in Figure 1B. The cylindrical pore electrode described above contains n such pores connected in parallel (26). This is the equivalent circuit describing an equal number of finite, parallel transmission lines

(25,34). Note that the faradaic branch found in the Randles circuit (containing $R_{ct}$ and $Z_w$) is absent from this circuit. The real and imaginary components of the impedance for this circuit are given by (25):

$$Z[re] = Ru + (\lambda/l)\frac{\sinh(\lambda/l) - \sin(\lambda/l)}{\cosh(\lambda/l) - \cos(\lambda/l)} \tag{15}$$

$$Z[im] = (\lambda/l)\frac{\sinh(\lambda/l) + \sin(\lambda/l)}{\cosh(\lambda/l) - \cos(\lambda/l)} \tag{16}$$

where l is the equivalent cylindrical pore length, and $\lambda$ is the penetration depth of the AC signal, given by (26):

$$\lambda = 1/2(r_c\sigma/\omega C_{dl})^{1/2} \tag{17}$$

Where $\sigma$ is the conductivity of electrolyte in the pores, $\omega$ is the angular frequency, $r_c$ is the equivalent cylindrical pore diameter, and $C_{dl}$ is the specific double-layer capacitance. With these equations, Nyquist diagrams can be generated for any desired set of electrode parameters.

Qualitatively, the Nyquist diagrams calculated from this equation are identical in shape to those generated by Eqs. 10 and 11 except for the absence of the charge transfer limited semi-circle. That is, a $45^o$ linear region is observed at high frequencies ($\lambda \ll 1$), and both the capacitance and resistance reach the limiting values $R_l$ and $C_l$ at low frequencies ($\lambda \gg 1$). However, the origin of the limiting behavior is different in the

present case than in Case I. The penetration depth of the AC signal (Eq. 17) into the pores of the metallic film is a function of $\sigma$, $C_{dl}$, $r_c$, and $\omega$. As the frequency decreases, l increases and a greater total pore volume with its associated resistance and capacitance are accessed. Thus, as predicted by Eqs. 15 and 16, increases in Z[re] and $(\omega Z[im])^{-1}$ are commensurate with decreasing $\omega$. At some sufficiently low frequency, $\lambda = 1$ and the total volume accessed by the AC signal approximately equals the total available pore volume. At this frequency, Z[re] and $(\omega Z[im])1-$ assume the limiting values $R_1$ and $C_1$.

If $C_{dl}$, $\sigma$, and l are known, the equivalent cylindrical parameters $r_c$ and n of the porous film can be calculated from $R_1$ and $C_1$ (26):

$$R_1 = \frac{1}{3n\ r_c^2} \tag{18}$$

$$C_1 = 2n\ r_c l C_{dl} \tag{19}$$

The pore length, l, and the volume of electrolyte in the pores of the film, Vp, are related by the expression:

$$l = (3R_1V_p\sigma)^{1/2} \tag{20}$$

As a consequence of this equation, either l or $V_p$ is sufficient when combined with $C_{dl}$, $\sigma$ and the experimental values Rl and Cl to calculate $r_c$ and n for a porous film (26).

## EXPERIMENTAL

*Materials and Equipment*

Platinum foil (t = 0.254 mm, Alfa) and extruded Kel-F rod (d = 0.5 in, Afton Plastics Molding) were used to construct Pt disk electrodes as follows. The Kel-F electrode body was first machined to the dimensions shown in Fig. 2. Pt disks (d = 3.3 mm) were then heat-sealed onto the surface of the Kel-F body by melting the Kel-F around the Pt disk with a heat gun and physically pressing the Pt disk into the heat-softened surface with a glass rod. Electrical contact was made to the back of the Pt disk with a copper wire and silver epoxy (Epo-Tek 410E, Epoxy Technology) as shown in Fig. 2. Excess Kel-F was removed from the surface of the Pt/Kel-F electrode by polishing with 400 grit and 600 grit Carbimet (Beuhler) paper until a planar electrode surface was established. This surface was then further polished sequentially with 1.0 $\mu$m, 0.3 $\mu$m, and 0.05 $\mu$m alumina powder (all from Buehler Inc.). After this initial polishing sequence, the electrode surface was polished between experiments with 0.05 $\mu$m alumina only.

A large area, Pt gauze counter electrode (25 x 25 mm, AESAR) and a conventional saturated calomel reference electrode (SCE) were employed for all electrochemical experiments.

Tetrabutylammonium tetrafluoroborate electrolyte was prepared from ammonium tetrafluoroborate (97+%, Aldrich) and tetrabutylammoniun bromide (99% Aldrich) and recrystalized from ethyl acetate-pentane. The recrystallized salt was dried envacuo at 100 C for ca. 24 hrs. prior to use. Pyrrole (98%, Aldrich) was distilled in an inert atmosphere and stored over

argon. Acetonitrile (Burdick and Jackson, UV Grade) was used as received. All solutions employed for electrochemical measurements were purged with purified $N_2$ prior to use.

A EG&G PAR Model 273 potentiostat/galvannostat was employed for film deposition and all electrochemical measurements. Cyclic voltammograms were recorded on a Houston Instruments Model 2000 X-Y recorder. AC impedance measurements were performed in conjunction with a computer controled EG&G Model 5301 Lockin Amplifier and EG&G AC impedance software. At frequencies greater than 5 Hz., the applied sine-wave excitation signal was generated and the current response analyzed by the lockin amplifier-controlled PAR 273. The measured impedances were then transfered to the computer for display and storage. At lower frequencies, the EG&G software removes the lockin amplifier from the circuit and the sine wave excitation signal is computer generated. The current response obtained from any desired number of cycles is measured by the 273, then analyzed by computer via a fast fourier transform (FFT) algorithm. At these lower frequencies, the impedance was determined from the data obtained from 3 cycles. The amplitude of the applied potential sine wave in each case was 10 mV. Calibration of the 5301 is accomplished automatically with internal standards. All impedance measurements were normalized to an electrode area of 1 $cm^2$.

The conductivity of 0.2 M $Bu_4NBF_4$, MeCN electrolyte was measured with a Yellow Springs Instruments Model 31 AC conductivity bridge and a conventional YSI parallel plate conductivity cell. The cell constant was determined with KCL solutions. All solutions were equilibrated in a 25 C water bath.

*Film Deposition and Electrochemical Measurments*

Polypyrrole films were prepared from monomer solutions containing 0.5 M pyrrole, 0.2 M $Bu_4NBF_4$ in acetonitrile. Polymerization was accomplished galvanostatically in a conventional one-compartment cell at a current density of 1.0 mA $cm^{-2}$. A polymerization charge of 0.10 C $cm^{-2}$ was found to correspond to an oxidized film thickness of 0.27 $\mu m \pm 0.02$ $\mu m$ as measured by a Tencor Alfa-Step profilometer. After deposition, the integrity of each polymer film was ascertained by recording a cyclic voltammogram at 20 mV/sec. All electrochemical measurments were conducted in $N_2$ purged, 0.2 M $Bu_4NBF_4$, acetonitrile electrolyte.

AC impedance data was obtained by first potentiostating the polymer at the desired potential for 60 seconds, then equilibrating the polymer at open circuit for 120 seconds. The polymer was then potentiostated at the terminal open circuit potential before AC impedance data acquisition was initiated. This procedure resulted in Nyquist diagrams which exhibited no hysteresis with varying potential. This indicates that the impedance data is obtained at each potential on polymer which is in equilibrium with the mean applied potential. The AC impedance was measured for each open circuit potential at 42 frequencies from 0.05 Hz. to 100 KHz.

## RESULTS AND DISCUSSION

Figure 3 shows a cyclic voltammogram in 0.2 M $Bu_4NBF_4$, MeCN electrolyte for a typical 0.27 $\mu m$ polypyrrole film employed for the AC impedance studies below. The large capacitive currents in the region positive of the polymer redox reaction ($E > +0.1$ V) indicate that the polymer is electronically conductive in its oxidized state. At potentials negative of ca. -0.3 V, the

capacitive currents decrease dramatically since the reduced polymer is an electronic insulator. The unusual, asymmetric shape of this voltammogram has been observed previously for thin polypyrrole films prepared and cycled in $Bu_4NBF_4$, MeCN electrolyte (36). As mentioned above, such cyclic voltammograms were routinely used to ascertain the quality of the polypyrrole films sythesized prior to performing the AC impedance experiments.

*Oxidized polypyrrole*

Theoretical Nyquist data for porous metallic films can be calculated for the film parameters $r_c$ and n from Eqs. 15 and 16 provided that $\sigma$, $C_{dl}$, and either l or $V_p$ are known. In the case of porous metal films, values for Vp are conveniently obtained gravimetrically from measurements of the water content of water impregnated films (26). This procedure, however, is impractical for the 0.27 $\mu$m polypyrrole films employed in this study since such films are too thin to be removed intact from the substrate electrode surface. For the purposes of estimating the parameters $r_c$ and n, then, $V_p$ was taken to be equal to the total film volume, $V_f = r^2 l$, and l was calculated from Eq. 20. An estimated value for $C_{dl}$ of 20 $\mu F\ cm^2$ was also employed based on the calculations of Feldburg (35). Again, this number which is typical of metal/electrolyte interfaces should be considered to be a limitingly high value. Because $r_c$ is proportional to both $C_{dl}$ and $V_p$, values for $r_c$ calculated from these estimates of $C_{dl}$ and $V_p$ should be considered maximum values.

Experimental and simulated Nyquist diagrams for polypyrrole at three open circuit potentials in the interval from +0.4 to +0.2 V are shown in

Figure 4. Figure 4A shows a comparison of the experimental data obtained at low frequencies ($f < 5$ Hz.). Note that at all three potentials, Z[re] is nearly frequency independent. As shown in Figure 5, plots of Z[im] (= $1/\omega C_s$) vs. $\omega^{-1}$ for this low frequency data are linear ($r > 0.999$) indicating that the capacitance is constant ($C_s = C_l$). Because this potential region is well positive of the polymer electrochemistry ($E^o = -0.2$ V), changes in the formal oxidation state of the polymer over this interval are small, ie. the polymer is essentially 100% oxidized at $E_{oc} > 0.2$ V. The similarity of the three plots shown in Figure 4A, then, corroborates the conclusion that the observed impedence is predominately nonfaradiac. Thus, Case II limiting behavior is observed.

Figures 4B - 4D show the high frequency Nyquist data in greater detail. Simulated plots were generated in each case by fitting to the experimental data using $r_c$ and n as adjustable parameters. The resulting best-fit values for these parameters are listed in Table I. Note that the agreement between the simulated and the experimental data is best at 0.393 V (Fig. 4B). In particular, at this potential the elbow in the Nyquist plot occurs at very similar frequencies; ca. 40 rad $sec^{-1}$ (expt.) vs. 25 rad $sec^{-1}$ (calc.). The values for $r_c$ and n of 4.26 A and $5.43 \times 10^{12}$ pores $cm^{-2}$ obtained from the simulation at 0.393 V (Table I) are reasonable limiting values in view of what is known about the morphology and mass transport characteristics of polypyrrole films. For example, as mentioned above, the data of Buttry and coworkers indicates that $Bu_4N^+$ with a crystallographic radius $r_{Bu_4N^+}{}^o = 4.75$ A (39) is excluded from polypyrrole during electrochemical oxidation/reduction cycles whereas $ClO_4^-$ ions ($r_{ClO_4^-}{}^o = 2.5$ A (39)) diffuse into and out of the film (30). In addition, scanning

electron micrographs (SEM) of polypyrrole obtained previously in this lab and by others (cf. 37,38) reveals that polypyrrole has an extremely dense, compact morphology. That individual pores or channels are not resolved by SEM indicates that any such structures must possess dimensions < ca. 50 A.

However, several important discrepancies between the experimental and the simulated data obtained at 0.393 V (Fig. 4B) are evident. Most noticeable are differences in the transistion from the high frequency 45° data to the low frequency limiting region. In contrast to the simulated data, the experimentally observed transition is more gradual; occurring over a band of frequencies from 10 - 60 Hz. Keiser and coworkers have determined that the exact shape of the Nyquist plot for a porous electrode is sensitive to the geometry of the pores (25). Their calculations for a variety of pore geometries predict that positive deviations in the Nyquist data relative to the cylindrical pore case are observed in the transition region for pores which possess a decreasing radius (25); ie., a pore radius less at the electrode end than at the electrolyte end. A similar positive deviation is observed for the data obtained at 0.276 V (Fig. 4C). This deviation may indicate that the mean pore diameter decreases as the polypyrrole film is traversed from the electrolyte/film interface to the electrode. Alternatively, this gradual transition may reflect the non-homogeneity of either $r_c$ or 1.

A second discrepancy relative to the simulated data is observed at frequencies above ca. 10 KHz. where Z[im] becomes negative. Experimental data in this frequency region was irreproducible from film to film. Negative Z[im] values at high frequencies reflect the presence of inductive effects which are not predicted by simple porous electrode theory (25,26).

Consequently, a more complex equivalent circuit may be required to thoroughly describe the electrical behavior of oxidized polypyrrole films.

The Nyquist data obtained at 0.186 V (Fig. 4D) shows evidence of a high frequency semi-circle which is characteristic of charge transfer limitations. The emergence of this feature in the Nyquist plot is expected as the polymer begins to be reduced (19,29). The faradaic component of the current present at this potential may augment the purely nonfaradiac current due to the porous electrode character of the film and contribute to the shift in $R_1$ which is observed (see intermediate data below). Thus, the equivalent circuit shown in Fig. 2B is not adaquate to describe polypyrrole at this potential and the fit of the simulated to the experimental data in Fig. 4D is poor.

Although no evidence for charge transfer limitations is observed at 0.276 V (Fig. 4C), the fit of this data to the cylindrical porous electrode model is intermediate to that of the 0.393 V data (Fig. 4B) and the 0.186 V data (Fig. 4D). For example, transition to the vertical limiting region occurs at ca. 40 rad $sec^{-1}$ (expt.) vs. 15 rad $sec^{-1}$ (calc). At lower frequencies, the experimental Z[im] data is significantly higher than that predicted from Eqs. 15 and 16.

The fact that the fit between the experimental and simulated data improves as the potential increases from 0.186 V to 0.393 V suggests further improvement might be observed at yet higher open circuit potentials. Unfortunately, irreversible oxidation begins to occur at potentials greater than ca. +0.5 V vs. SCE and reliable AC data in this region cannot be obtained. However, the above data shows that the AC impedance of oxidized polypyrrole can be modeled reasonably well with an extremely simple finite,

porous electrode model which assumes a cylindrical pore geometry. Again, a better fit to the experimental data is possible if a decreasing radius pore geometry is considered. Nyquist diagrams for such films are easily calculated numerically using the procedure of Keiser et al. (25).

*Lightly doped polypyrrole*

Figure 6 shows experimental and simulated Nyquist diagrams for polypyrrole at open circuit potentials of -0.333V, -0.35V, and -0.361 V. As the cyclic voltammogram in Figure 3 shows, these potentials are at the foot of the polymer oxidation wave. Since these potentials are well negative of $E^{o\prime}$ ($|E^{o\prime} - E_{oc}| > 150$ mV), the concentration of oxidized sites, $C_{PPy+}$ (where $C_{PPy+} = C_{BF4-}$), or the % doping of the polymer ought to be small. As discussed above, the data of previous workers (27,28) and the capacitance data of the present paper indicates that increases in the conductivity of polypyrrole at these $E_{oc}$ values are small, ie. the polymer film is essentially nonconductive. Thus, the AC response of the system ought to conform to Limiting Case I.

Figure 6A shows the experimental low frequency Nyquist plots at these three potentials. Note that Z[re] is nearly frequency independent for $f < 5$ Hz and limiting behavior similar to that observed for oxidized polypyrrole is seen. Plots of Z[im] vs. $\omega^{-1}$ at these frequencys are linear ($r > 0.999$) again showing that a constant, limiting low frequency capacitance obtains. Such limiting behavior is accounted for in Limiting Case I by a finite RC transmission line (Fig. 2A) where the nonfaradaic circuit components of the oxidized polymer circuit (Fig. 2B) are replaced by the charge transfer resistance, $R_{ct}$, the Warburg resistance, $R_w$, and the Warburg capacitance,

$C_W$. In addition, the capacitance of the Pt substrate electrode, which was assumed to be negligible in the oxidized polymer case, must be accounted for in Limiting Case I since the total double-layer capacitance of the system is small.

Figures 6B - 6D compare the experimental data obtained at higher frequencies with simulated Nyquist plots. Simulated data calculated from Eqs. 10 and 11 were fit to the experimental data using the diffusion coefficient, $D_{BF_4^-}$, and the gradient of the potential with respect to the concentration, $dE/dC_{BF_4^-}$. The values of these parameters (see Table II) are identical to those calculated from the experimental R1 and C1 using Eqs. 13 and 14. Note that the agreement between the experimental and the simulated data at all three potentials is good. The best-fit diffusion coefficients obtained from the simulation of ca. $1 \times 10^{-9}$ $cm^2$ $sec^{-1}$ are approximately an order of magnitude faster than those measured by Genies and coworkers for polypyrrole ($D = 2.3 \times 10^{-10}$ $cm^2$ $sec^{-1}$ in $Et_4NBF_4$, MeCN) using chronoamperometry (40). As discussed above, this disparity is not unexpected in view of the very different nature of these two experiments; ie., in the potential step (Cottrell) experiment, diffusion coefficient information is obtained while the film is in flux from one redox state to another (29). However, the diffusion coefficients obtained here are in agreement with those obtained at identical films and potentials by small-amplitude current pulse experiments (41).

Diffusion coefficients can also be calculated from the semi-infinite diffusion region of the Nyquist data. Figure 7A shows the experimental Nyquist plots obtained in this region in greater detail. The slopes calculated from these data (Table II) are in close agreement with the

theoretically predicted slope of unity. Plots of the impedance modulus, $|Z|$, versus $\omega^{-1/2}$ for this frequency domain are shown in Figure 7B. The diffusion coefficient can be calculated from these data by using values for $dE/dC_{BF_4^-}$ obtained from the finite diffusion region (Table II) and Eq. 12. The values for $D_{BF_4^-}$ so obtained (Table II) are smaller at each potential than those calculated from the finite diffusion frequency domain; $(D_{SI}/D_F)_{-0.333} = 0.28$, $(D_{SI}/D_F)_{-0.350} = 0.31$, $(D_{SI}/D_F)_{-0.361} = .28$. Note that $D_{SI}/D_F$ is ca. 0.3 at all three potentials. Rubinstein et al. have observed similar behavior for the AC impedance of the reversible redox couple $Ru(bpy)_3^{3+/2+}$ in Nafion modified electrodes (20). At Nafion modified electrodes, however, diffusion coefficients obtained from the semi-infinite diffusion region are <u>faster</u> by a factor of ca. 3 than those obtained from the finite diffusion limiting region.

The factors which might account for the observed discrepancy between $D_{SI}$ and $D_F$ in the polypyrrole films studied here are identical to those discussed in detail by Rubinstein and coworkers (20). Note that an additional complication in the case of polypyrrole is the estimation of $dE/C_{BF_4^-}$ which cannot be determined by a straightforward coulometric titration without a reliable double-layer capacitance correction. Consequently, the value of $dE/dC_{BF_4^-}$ employed here is that derived from the finite diffusion data. The simultaneous determination of $dE/dC_{BF_4^-}$ and $D_{F,BF_4^-}$ is susceptible to error from film thickness nonuniformity. However, because the thickness of the films used here is known to be 0.27 $\mu$m $\pm$ 0.02 $\mu$m, film nonuniformity seems an unlikely source of the diffusion coefficient effect.

The possibility exists, however, that the <u>morphology</u> of the polypyrrole

film is nonuniform over the film thickness. Under these circumstances, $D_{SI}/D_F < 1$ would be produced by a film morphology which was dense (transport restrictive) at the electrode/film interface and relatively open at the film/electrolyte interface. It is interesting to note that the existence of such a morphological gradient could also explain the AC impedance data obtained for the oxidized polymer (see explanation above). Furthermore, it is not unlikely that such gradients in the polymer void volume or effective pore diameter might be introduced during electrochemical synthesis of the polymer film. This is particularly true since the polypyrrole polymerization reaction is not diffusion controlled at the current densities employed here (1 mA $cm^{-2}$)(40). Thus, pyrrole monomer is available at the film edge and the polymerization reaction can proceed from the interior surfaces of the film as well as at its exterior (apparent) surface. As a result, the total time available for polymerization at the interior surfaces of the film increases from the film/monomer interface to the electrode. The effective pore diameter of the electrochemically synthesized film, then, increases from the electrode surface to the film edge. It should be noted that although a morphological gradient in the polypyrrole film such as that described above is consistent with the observed AC impedance data, alternative explanations exist. For example, Rubinstein et al. have accounted for the similar effects observed at Nafion-coated electrodes with a model which incorporates two uncoupled parallel diffusion pathways (20).

A second similarity between the present data and that of Rubinstein et al. is the behavior of the experimental data in the transition region (23). As shown in Figs. 4B - 4D, experimental Nyquist plots exhibit a gradual

transition from the semi-infinite ($45^{o}$) to finite (vertical) diffusion regions of the Nyquist plot whereas a relatively abrupt transition is predicted by Eqs. 10 and 11. This effect is probably best attributed to inhomogeneities in the polymer structure which result in a distribution of diffusion pathways (apparent film thicknesses).

*Intermediate oxidation levels.*

At potentials from -0.3 V to +0.1 V, significant concentrations of both oxidized and reduced polymer are present in a film which is also a good electronic conductor. Under these circumstances, neither of the equivalent circuits employed above are adequate to describe the AC impedance of the polymer. The faradaic impedance of porous electrodes has been discussed in detail by De Levie (32-34). The proposed models, however, do not consider the finite diffusion case and become complex if the effective pore diameter approaches dimensions of ca. 1 $\mu$m (34). In addition, the modeling of polypyrrole at these intermediate potentials is complicated by the need to know the specific double layer capacitance (or the true surface area) of the polymer at each potential. More sophisticated porous electrode models (cf. 42,43) introduce additional adjustable parameters which are difficult to experimentally identify. Finally, it should be noted that the work of Feldburg (35) and others suggests that significant extensions of established porous electrode theory are likely to be neccessary to fully account for the AC impedance behavior of conducting polymers.

Although we have not attempted to identify an equivalent circuit appropriate for the AC data obtained at intermediate potentials, important qualitative data can be obtained in the absence of such a model. Figure 8

shows Nyquist plots for AC impedance data obtained at potentials from +0.1 V to -0.3 V vs. SCE. The low frequency data (Figs. 8A and 8B) show that these data are qualitatively similar to that which was observed at more positive and more negative potentials. Both the capacitance and the resistance assume limiting values, $R_l$ and $C_l$, at frequencies less that 5 Hz. A plot of $R_l$ and $C_l$ vs. $E_{oc}$ obtained over the entire potential region from +0.4 V to -0.3 V is shown in Figure 9. Note in particular that the capacitance in the region from -0.3 V to -0.4 V is small relative to the maximum $C_l$ values observed at higher potentials; ie., for the fully oxidized polymer. This data supports our assumption (Limiting Case I) that polypyrrole-$BF4^-$ is relatively nonelectronically conducting at these potentials. The value of $C_l$ for the oxidized polymer (3 x 10-2 F $cm^{-2}$ @ $E_{oc}$ = 0.393 V)) corresponds to a bulk capacitance of 350 F $cm^{-3}$. This number is significantly higher than that observed by Burgemayer et al. (200 F $cm^{-3}$ (2)) and by Diaz et al. (100 F $cm^{-3}$ (36)). Note also that for $C_l$, a maximum is observed at ca. -0.2 V. These data are similar to that obtained by Tanguy et al. for thick polypyrrole films (13,14). In the vicinity of the switching potential ($E^{o\prime}$) both the faradaic components ($R_{l,f}$ and $C_{l,f}$) and the capacitive components ($R_{l,c}$ and $C_{l,c}$) of $R_l$ and $C_l$ are expected to be significant.

To a first approximation, the limiting low frequency behavior of these components $R_l$ and $C_l$ can be inferred by superimposing the predictions of Limiting Case I (Eqs 13,14) and Limiting Case II (Eqs. 18,19). If the specific double layer capacitance, $C_{dl}$, of polypyrrole can be assumed to possess an S-shaped dependence with potential (no maximum), Eq. 19 predicts that if $r_c$ and l remain constant, $C_{l,c}$ vs. $E_{oc}$ will have a similar shape. In this case, since the faradaic component, $C_{l,f}$, is a maximum at $E_{oc}$ =

$E^{o\prime}$(24), the superposition of faradaic and capacitive components yields a Cl vs. Eoc relation which has a maximum near Eo', as observed here and previously (13,14). Equation 13 predicts that the faradaic component $R_{l,f}$ ought to be a minimum at $E_{oc} = E^{o\prime}$. Thus, it is difficult to account for the potential dependence of $R_l$ observed here. Since the capacitive component, $R_{l,c}$ is proportional to 1, $\sigma^{-1}$, and $r_c^{-2}$ (Eq. 19), relatively dramatic changes in the pore structure (eg. increases in $r_c$ with potential) are probably neccessary to account for the $R_l$ vs. $E_{oc}$ relationship obtained by us and by previous workers (13,14).

Figure 8C,D shows the high frequency Nyquist data obtained at intermediate potentials. Of particular interest is the absence of a well defined semi circle resulting from charge transfer limitations at high frequencies (26,29). The AC impedence data obtained by various workers (2,13) for thick films invariably reveals the presence of such a semi-circle at high frequencies. Unfortunately, quantitative measurement of the heterogeneous rate constant for this system is impossible given the porous electrode nature of the film; ie., the electroactive area of the film is not well defined. However, the present data suggests that the apparent rate constant may decrease considerably with increasing film thickness.

The high frequency resistance, $R_h$, obtained at Z[im] = 0 is compared to $C_l$ in Figure 10. $R_h$ values are good approximations of the total series resistance of the solution and the polypyrrole film (29). The $R_h$ values observed at positive potentials ($R_h$ = 6.5 ohms $\pm$ 0.2 ohms) can be attributed entirely to the supporting electrolyte resistance; ie., the film resistance of the oxidized polymer is negligible. At potentials negative of -0.2 V, $R_h$ increases rapidly to ca. 20 ohms at -0.6 V. It is interesting to note that

decreases in $R_h$ commensurate with oxidation of the polymer film occur in advance of increases in $C_l$. Note, for example, that at -0.3 V, the value of $R_h$ is 15% of its value at -0.6 V whereas $C_l$ has only attained ca. 15% of its limiting value. Since the value of $C_l$ is sensitive only to the electronic conductivity of the film whereas that of $R_h$ can reflect either ionic or electronic conductivity, these data suggest that polypyrrole is a good ionic conductor at potentials (near -0.3 V) where it is a relatively poor electronic conductor.

## Conclusions

AC impedance data has been presented for thin polypyrrole film-modified electrode surfaces. Although an equivalent circuit which accounts for the observed AC behavior of polypyrrole over a wide range of potentials is likely to be complex, two limiting cases exist for which the equivalent circuits are simplified. At low doping levels (Limiting Case I), the equivalent circuit appropriate for polypyrrole is identical to that used previously to describe the AC impedance of Nafion polymer modified electrodes (20,24) and metal oxide, Li intercalation films (19,21-23). Diffusion coefficients were obtained from the analysis of Ho et al. (19) for both semi-infinite and finite time domains. The approximate ratio of the values $D_{SI}/D_F = 0.3$ at the potentials examined. This observation is consistant with the existence of a morphology gradient normal to the surface of the electrode where the effective pore diameter of the polymer, and therefore the diffusion coefficient $D_{BF_4^-}$, increases in the film with distance from the electrode surface.

The AC impedance data observed for the oxidized polymer (Limiting Case

II) was compared to that predicted for finite, porous metallic films (25,26). The agreement between the experimental and the simulated Nyquist data (calculated from ref. 26) improves with increasing $E_{oc}$. Using the analysis of Candy and coworkers, film parameters such as the pore radius, pore length, and pore number density can be expressed as their cylindrical pore electrode equivalents (26). The values so obtained for thin polypyrrole films are consistant with what is currently known about mass transport in such films. Better agreement between the simulated and the experimental Nyquist plots ought to be obtained if other pore geometries are considered. In particular, the transition region of the Nyquist data is better accomodated by a model in which the pores possess a decreasing radius from the film edge to the electrode surface. This conclusion is in qualitative agreement with the diffusion coefficient data obtained for the oxidized polymer.

Thus, both mass transport and structural information can be gleaned from AC impedance analysis of polypyrrole films based on these two relatively simple equivalent circuits. In addition, the potential dependence of the low frequency series resistance and capacitance were determined and the origins of the observed dependencies were discussed. Comparisons between the high frequency resistance and the low frequency capacitance indicate that significant ionic conductivity is present for polypyrrole films at very low oxidation levels, prior to the onset of significant electronic conductivity.

**Acknowledgments**

The authors express appreciation to R.E. White for the use of the AC impedance instrumentation employed in this work.

**Credit**

This work was suported by the Office of Naval Research, the Robert A. Welch Foundation, the Air Force Office of Scientific Research, and NASA.

## References


1. P. Burgmayer and R.W. Murray, *J. Am. Chem. Soc.*, **104**, 6139 (1982).
2. P. Burgmayer and R.W. Murray, *J. Phys, Chem.*, **88**, 2515 (1984).
3. F. Garnier, G. Tourillon, M. Gazard, and J.C. Dubois, *J. Electroanal. Chem.*, **148**, 299 (1983).,
4. M. Gazard, in "Handbook of Conducting Polymers, Volume 1," Marcel Dekker, Inc., New York, 1986, p. 673.
5. J.H. Kaufman, T.-C. Chung, A.J. Heeger, and F. Wudl, *J. Electrochem. Soc.*, **131**, 2092 (1984).
6. N. Mermilliod, J. Tanguy, and F. Petiot, *J. Electrochem. Soc.*, **133**, 1073 (1986).
7. P. Button, J. Mastragostino, S. Panero and G. Scrosati, *Electrochimica ACTA*, **31**, 783 (1986).
8. F. Trinidad, J. Alonso-Lopez, and M. Nebot, *J. App. Electrochem.*, **17**, 215 (1987).
9. S. Chao and M.S. Wrighton, *J. Am. Chem. Soc.*, **109**, 2197 (1987).
10. E.P. Lofton, J.W. Thackeray, and M.S. Wrighton, *J. Phys. Chem.*, **90**, 6080 (1986), and references therein.
11. M. Josowicz and J. Janata, Anal. Chem., **58**, 514 (1986).
12. T. Osaka, K. Naoi, S. Ogano, and S. Nakamura, *Chem. Lett.*, 1687 (1986).
13. J. Tanguy, N. Mermilliod, and M. Hoclet, *J. Electrochem. Soc.*, **134**, 795 (1987).
14. J. Tanguy, N. Mermilliod, and M. Hoclet, *Syth. Met.*, **18**, 7 (1987).
15. A.F. Diaz, J.I. Castillo, J.A. Logan, and W.-Y. Lee, *J. Electroanal. Chem.*, **129**, 115 (1981).

16. G.B. Street, T.C. Clarke, M. Krounbi, K. Kanazawa, V. Lee, P. Pfluger, J.C. Scott, and G. Wieser, *Mol. Cryst. Liq. Cryst.*, **83**, 253 (1982).

17. R.A. Bull, F-R. F. Fan, and A.J. Bard, *J. Electrochem. Soc.*, **129**, 1009 (1982).

18. S.H. Glarum and J.H. Marshall, *J. Electrochem. Soc.*, **134**, 142 (1987).

19. C. Ho, I.D. Raistrick, and R.A. Huggins, *J. Electrochem. Soc.*, **127**, 343 (1980).

20. I. Rubinstein, J. Rishpon, and S. Gottesfeld, *J. Electrochem. Soc.*, **133**, 729 (1986).

21. D.R. Franceschetti and J.R. MacDonald, *J. Electrochem. Soc.*, **101**, 307 (1979).

22. D.R. Franceschetti and J.R. MacDonald, *J. Electrochem. Soc.*, **129**, 1754 (1982).

23. D.R. Franseschetti, *J. Electroanal. Chem.*, **178**, 1 (1984).

24. C. Gabrielli, O. Haas, and H. Takenouti, *J. App. Electrochem.*, **17**, 18 (1987).

25. H. Keiser, K.D. Beccu, and M.A. Gutjahr, *Electrochimica ACTA*, **21**, 539 (1976).

26. J-P. Candy, P. Fouilloux, M. Keddam and K. Takenouti, *Electrochimica ACTA*, **26**, 1029 (1981).

27. B.J. Feldman, P Burgemayer, and R.W. Murray, *J. Am. Chem. Soc.*, **107**, 872 (1985).

28. G.R. Kittlesen, H.S. White, and M.S. Wrighton, *J. Am. Chem. Soc.*, **106**, 7389 (1984).

29. A.J. Bard and L.R. Faulkner, "Electrochemical Methods: Theory and Applications," John Wiley & Sons, New York, 1980, p. 350.

30. D.A. Buttry, personnal communication, June, 1987.

31. J.E.B. Randles, *Disc. Faraday Soc.*, 1, 11 (1947).

32. R. De Levie, *Electrochimica ACTA*, **8**, 751 (1963).

33. R. De Levie, *Electrochimica ACTA*, **9**, 1231 (1964).

34. R. De Levie, in "Advances in Electrochemistry and Electrochemical Engineering," Chapt. 6, John Wiley & Sons, New York, 1967.

35. S.W. Feldburg, *J. Am. Chem. Soc.*, **106**, 4671 (1984).

36. A.F. Diaz, J.I. Castillo, J.A. Logan, and W.Y. Lee, *J. Electroanal. Chem.*, **129**, 115 (1981).

37. A.F. Diaz, W-Y. Lee, A. Logan, D.C. Green, *J. Electroanal. Chem.*, **108**, 377 (1980).

38. A.F. Diaz, *Chemical Scripta*, **17**, 145 (1981).

39. B. Kratochvil and H.L. Yeager, "Topics in Current Chemistry," Vol. 27, Springer Verlag, New York, 1972, p. 45.

40. E.M. Genies, G. Bidan, and A.F. Diaz, *J. Electroanal. Chem.*, **149**, 101 (1983).

41. R.M. Penner, L.S. Van Dyke, C.R. Martin, manuscript in preparation.

42. M. Tomkiewicz, *J. Electrochem. Soc.*, **126**, 2221 (1978).

43. M. Hepal and M. Tomkiewicz, *J. Electrochem. Soc.*, **131**, 1288 (1984).

**Table I. Summary of Film Parameters Calculated From AC Impedance Data For Oxidized Polypyrrole.**

| $E_{oc}$ (V vs. SCE) | equivalent cylindrical pore radius[a] (cm) | pore number density[a] ($cm^{-2}$) | pore length[b] (cm) |
|---|---|---|---|
| 0.393 | $4.26 \times 10^{-8}$ | $5.43 \times 10^{12}$ | $8.72 \times 10^{-4}$ |
| 0.276 | $2.63 \times 10^{-8}$ | $1.23 \times 10^{13}$ | $1.01 \times 10^{-3}$ |
| 0.186 | $1.96 \times 10^{-8}$ | $1.90 \times 10^{13}$ | $1.17 \times 10^{-3}$ |

[a]Values for $r_c$ and n were determined by fitting Nyquist plots calculated from Eqs. 15 and 16 to the experiment data. The values of $C_l$ used for these calculations were obtained from the slope of $Z[im] = (\omega C_s)^{-1}$ vs. $\omega^{-1}$ at $f < 5$ Hz. $R_l$ was determined from Z[re] at ca. f = 1 Hz. and corrected for $R_u$.

[b]Calculated from Eq. 20 assuming the pore volume $V_p$ = the total film volume, $V_f$.

**Table II. Summary of Transport Data Calculated For Semi-Infinite (SI) and Finite (F) Frequency Regimes For Lightly Doped Polypyrrole.**

| $E_{oc}$ (V vs. SCE) | $D_F$[a] ($cm^2\ sec^{-1}$) | $dE/dC$[a] ($V\ cm^3\ mol^{-1}$) | $d\|Z\|/d(\omega^{-1/2})$[b] (ohms $rad^{-1}$ sec) | $D_{SI}$[c] (cm2 sec-1) |
|---|---|---|---|---|
| -0.333 | $1.40 \times 10^{-9}$ | 593 | 1.36 | $3.87 \times 10^{-10}$ |
| -0.350 | $3.31 \times 10^{-9}$ | 1140 | 1.02 | $1.03 \times 10^{-9}$ |
| -0.361 | $3.38 \times 10^{-9}$ | 1300 | 1.20 | $9.36 \times 10^{-10}$ |

[a]Obtained by fitting Nyquist data calculated from Eqs. 10 and 11 to the experiment Nyquist data at each potential. The best fit values $D_F$ and dE/dC so obtained approximate those obtained from $R_1$ and $C_1$ and Eqs. 13 and 14.

[b]Obtained from the slope of the 45° linear region of the Nyquist plots shown in Fig. 7A.

[c]Calculated from $d|Z|/d(\omega^{-1/2})$ using Eq. 12.

## Figure Captions

Figure 1 - A. Randel's equivalent circuit with a finite Warburg element, $Z_{w,F}$. (19), B. Finite RC transmission line circuit equivalent to that of a finite pore with a uniform radius (ex. a cylindrical pore).

Figure 2 - Schematic diagram of the platinum disk electrode employed in this work. a. 7mm glass tube, b. copper wire, c. Kel-F electrode body; diameter = ca. 10 mm, d. silver epoxy contact, e. Pt disk; diameter = 3.3 mm.

Figure 3 - Cyclic voltammogram for a typical 0.27 $\mu$m polypyrrole film in 0.2 M $Bu_4NBF_4$, MeCN electrolyte at 20 mV $sec^{-1}$.

Figure 4 - A. Nyquist diagram comparing the low frequency ($f < 0.25$ Hz.) AC impedance data obtained at three potentials for an oxidized polypyrrole film. ○ - 0.393 V, ● - 0.286 V, △ - 0.186 V. Frequencies in Hz. are as shown.

B-D. Nyquist diagrams comparing experimental and simulated AC impedance data for an oxidized polypyrrole film. Frequencies (Hz.) for simulated data (solid line) are indexed on the right of each plot. Frequencies for the experimental data (open circles) are indexed at the left of each plot.

A. 0.393 V, B. 0.286 V, C. 0.186 V.

Simulated data calculated from Eqs. 15 and 16.

Figure 5 - Typical plot of Z[im] vs. $\omega^{-1}$ for data obtained at low frequencies. These data at f < 5 Hz. and 0.393 V.

Figure 6 - A. Nyquist diagrams comparing the low frequency AC impedance behavior at three potentials for a lightly doped polypyrrole film. ○ - -0.333 V, △ - -0.350 V, ● - -0.361 V.

B-D. Comparisons of experimental and simulated Nyquist diagrams. Frequencies (Hz.) for simulated data (solid line) are indexed on the right of each plot. Experimental data (open circles) are indexed at the left of each plot. A. -0.333 V, B. -0.350 V, C. -0.361 V.

Figure 7 - A. Comparison of the 45° semi-infinite region of the Nyquist data obtained for a lightly doped polypyrrole film. The slopes calculated for these plots are listed in Table II.

○ - -0.333 V, ● - -0.350 V, △ - -0.361 V.

B. Plots of |Z| vs. $\omega^{-1/2}$ for the linear regions of the plots shown in Fig. 7A.

□ - -0.333 V, △ - -0.350 V, ○ - -0.361 V.

Figure 8 - A,B. Comparison of experimental Nyquist data obtained at low frequencies for potentials from +0.1 V to -0.3 V. Frequencies in Hz. as shown.

A. ○ - 0.093 V, ● - 0.001 V, △ - -0.091 V, ▲ - -0.140 V.

B. ○ - -0.211 V, ● - -0.255 V △ - -0.299 V.

Figure 8 - C.D. Comparison of higher frequency experimental Nyquist data obtained at the same potentials. Identity of plots same as for Fig. 8 A,B. Frequencies in Hz. as shown.

Figure 9 - Low frequency resistance, $R_l$, and capacitance, $C_l$, vs. $E_{oc}$. $R_l$ measured at 0.25 Hz., $C_l$ obtained from plots of Z[im] vs. $\omega^{-1}$.

Figure 10 - High frequency resistance, $R_h$, and low frequency capacitance, $C_l$, vs. Eoc. $R_h$ = Z[re] at Z[im] = 0.

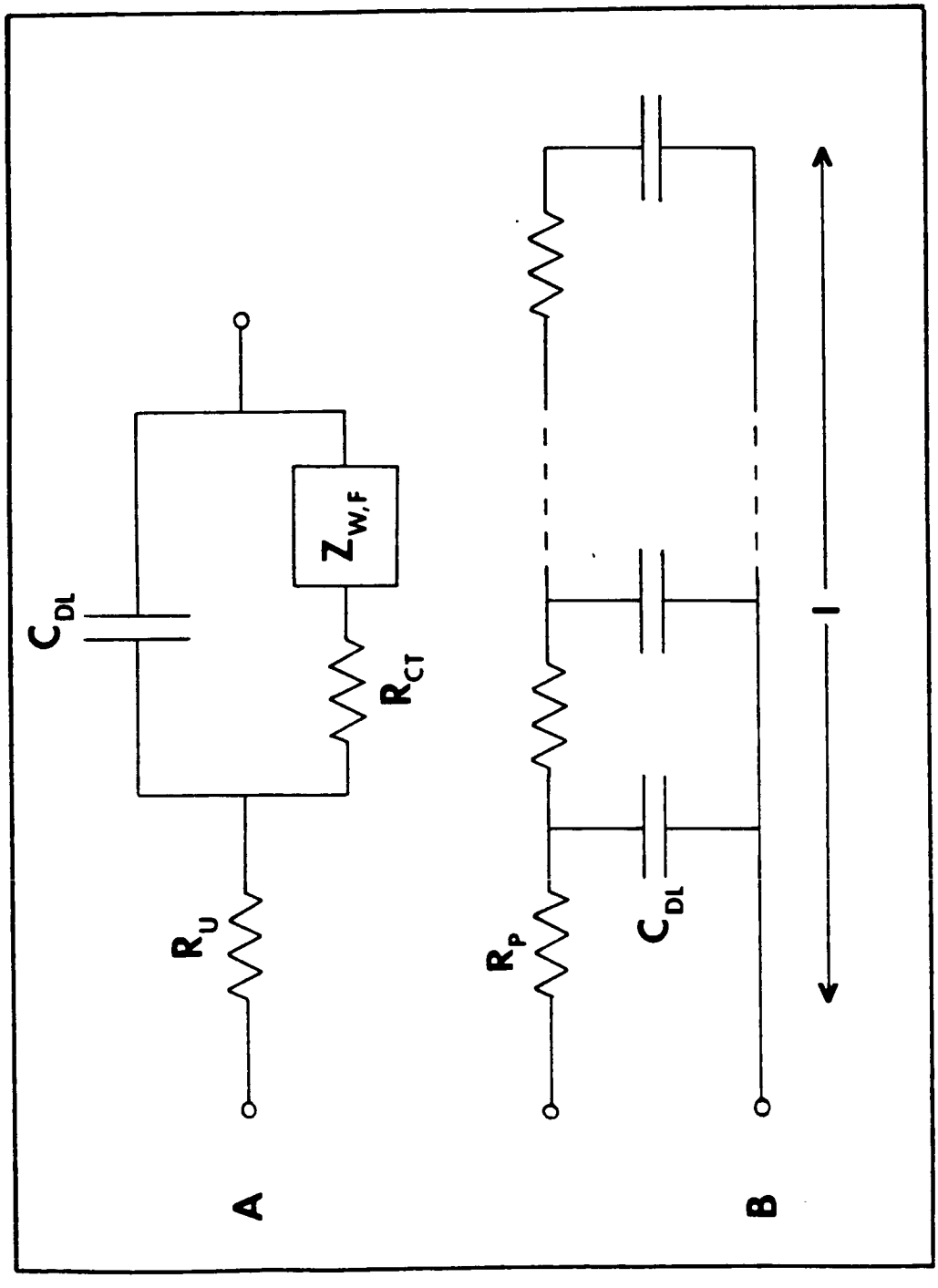


FIGURE 1

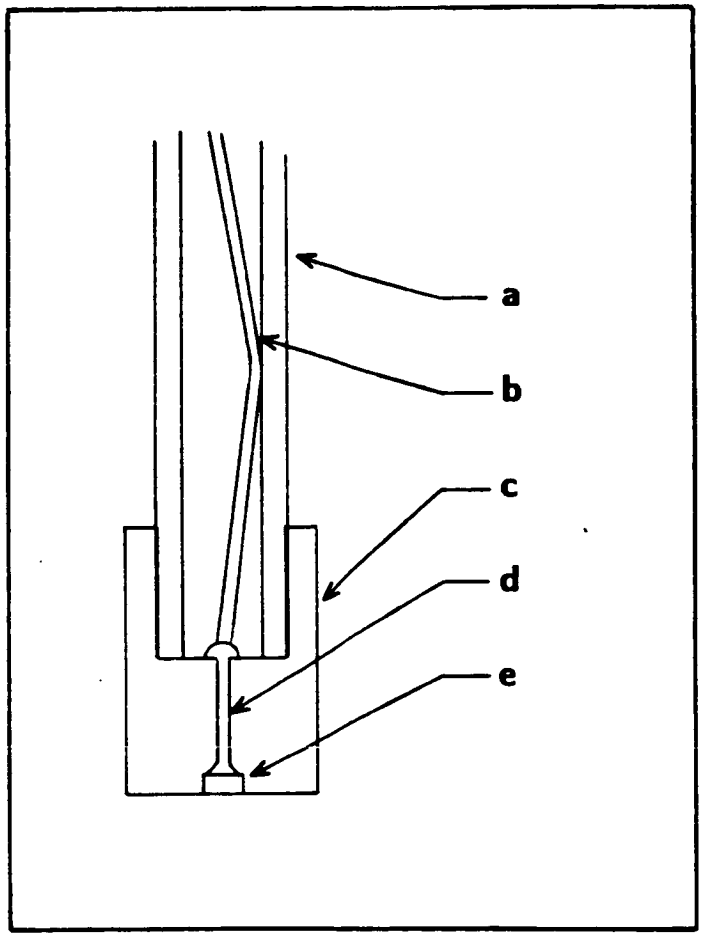


Figure 2

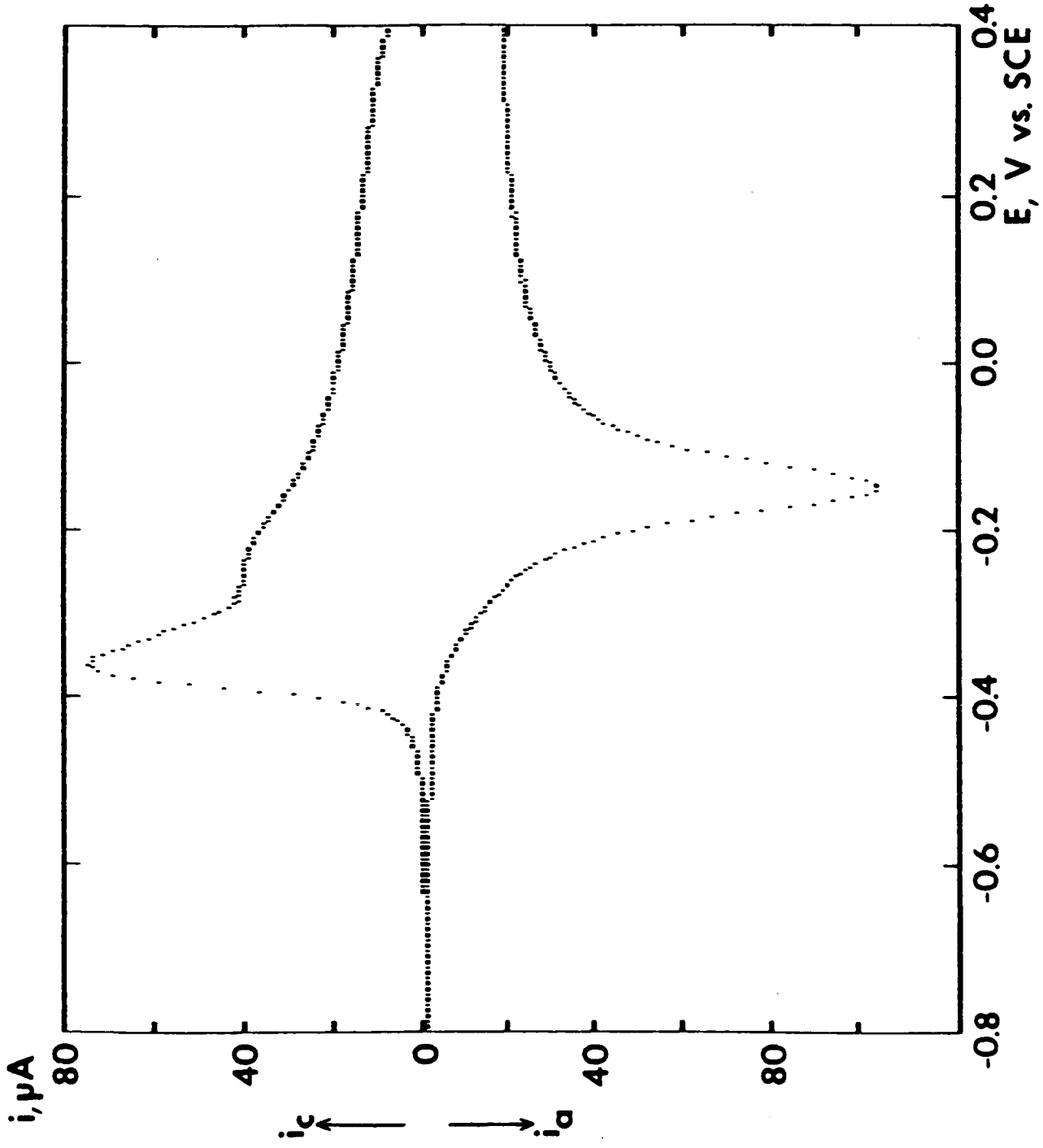


Figure 3

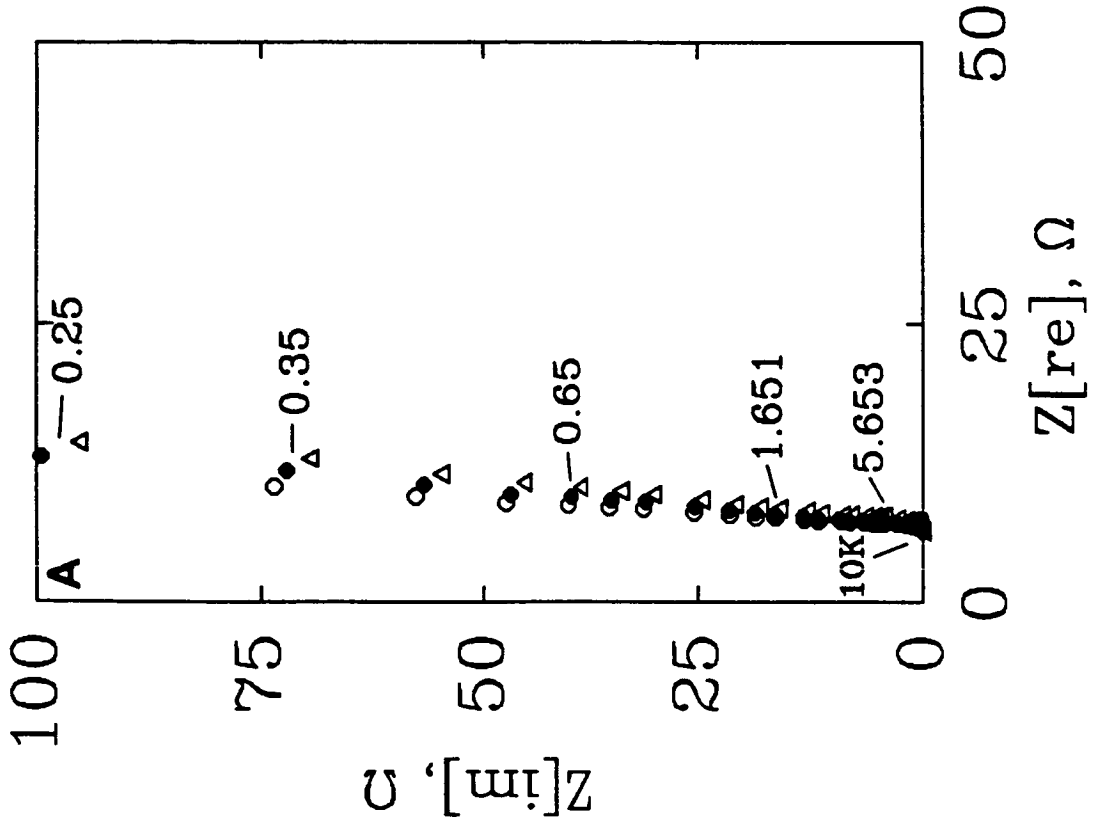


Figure 4-A

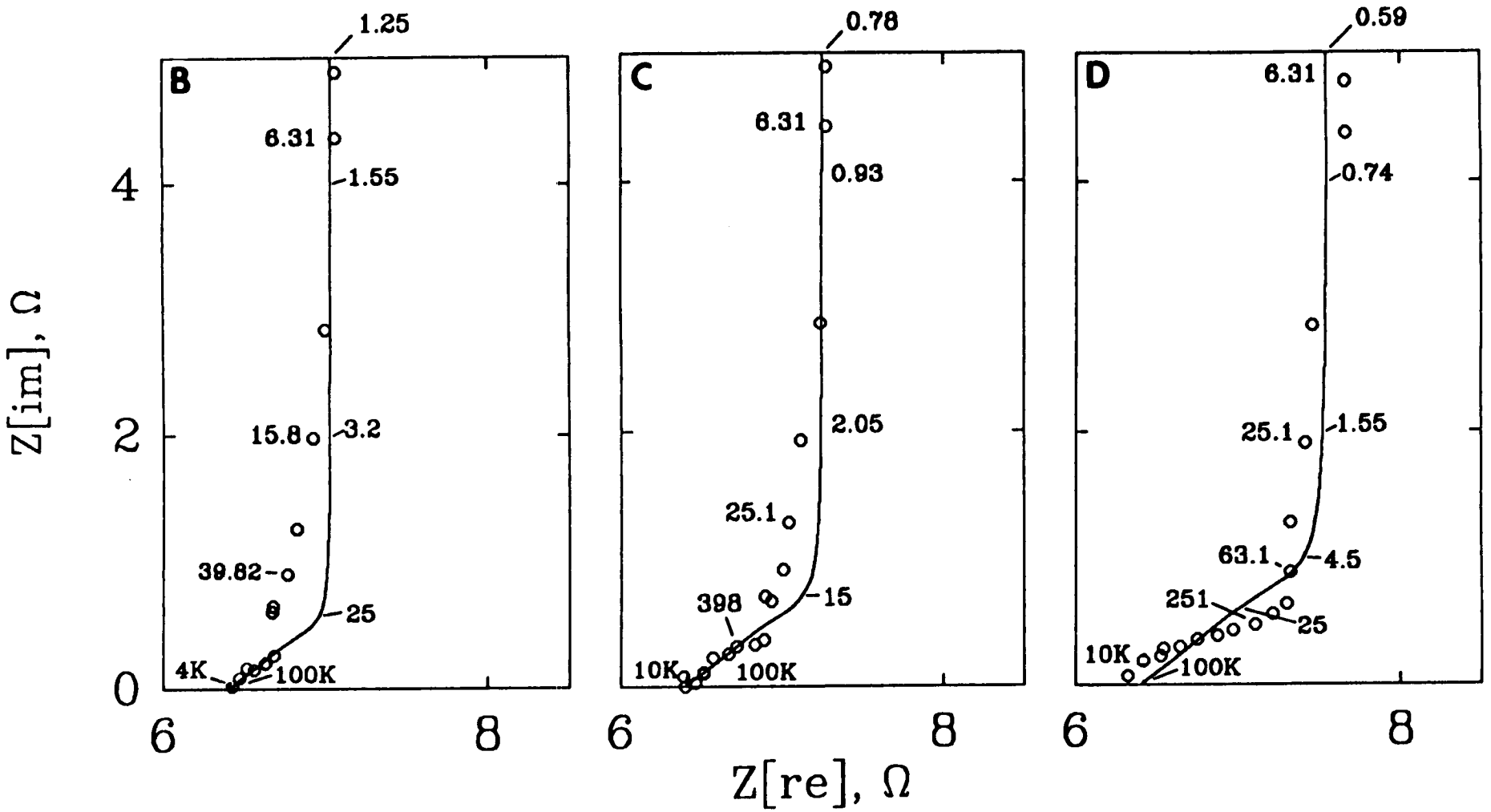
B
C
D
1.25
6.31
1.55
3.2
15.8
39.82
25
4K
100K
0.78
6.31
0.93
2.05
25.1
398
15
10K
100K
0.59
6.31
0.74
25.1
1.55
63.1
4.5
251
25
10K
100K
Z[im], Ω
Z[re], Ω
0
2
4
6
8

Figure 4-B,C,& D

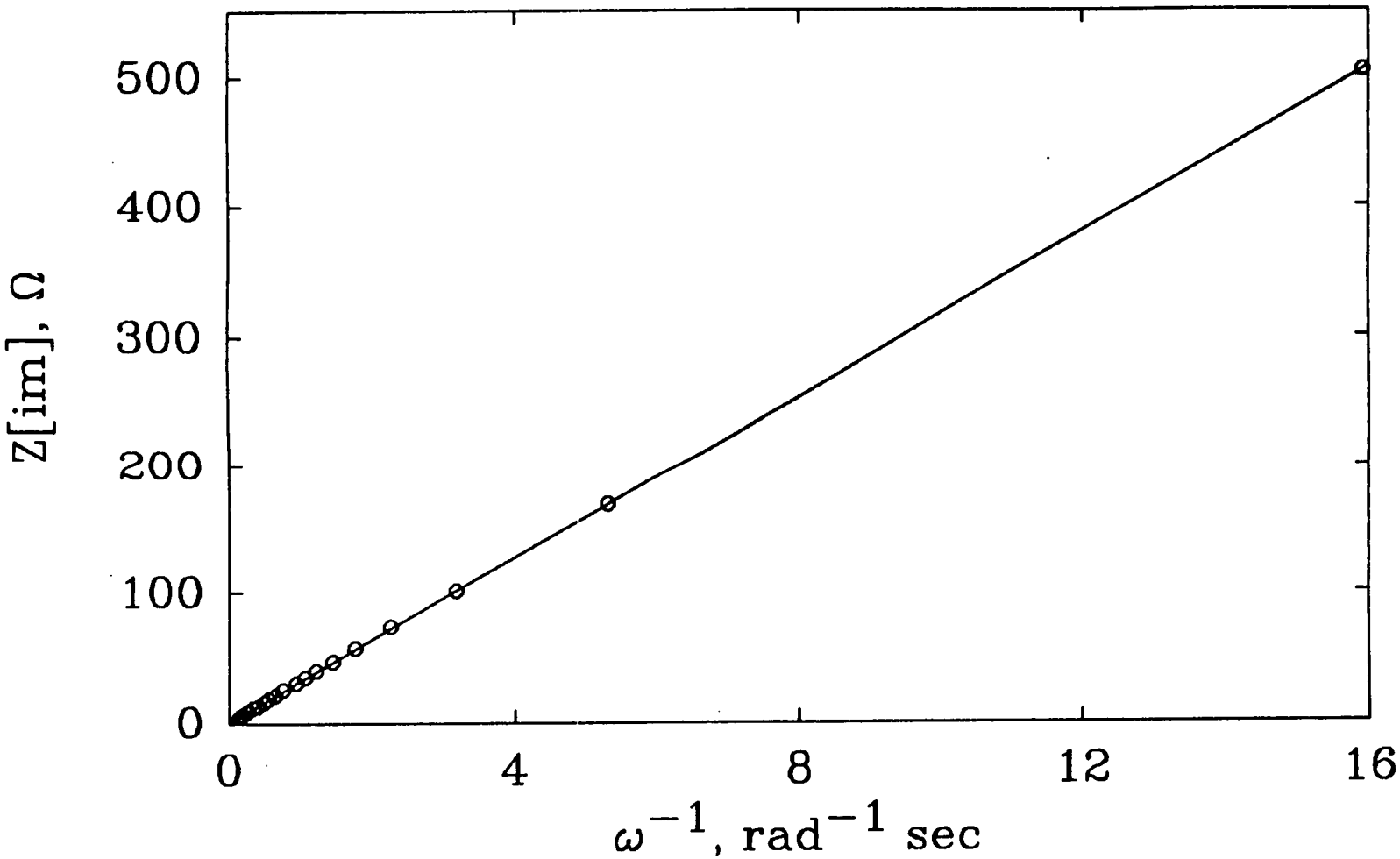


Figure 5

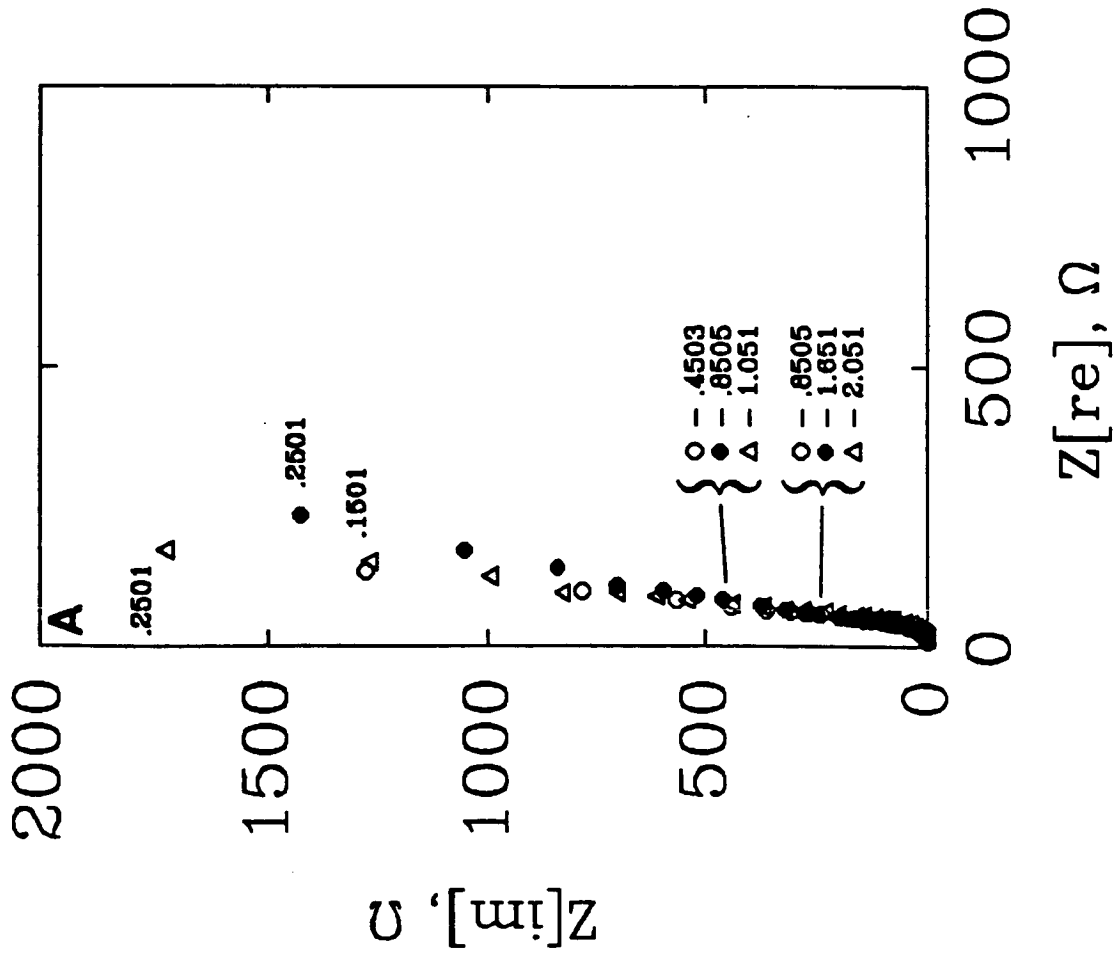
A
.2501
.2501
.1501
.4503
.8505
1.051
.8505
1.851
2.051
2000
1500
1000
500
0
0
500
1000
Z[im], Ω
Z[re], Ω

Figure 6-A

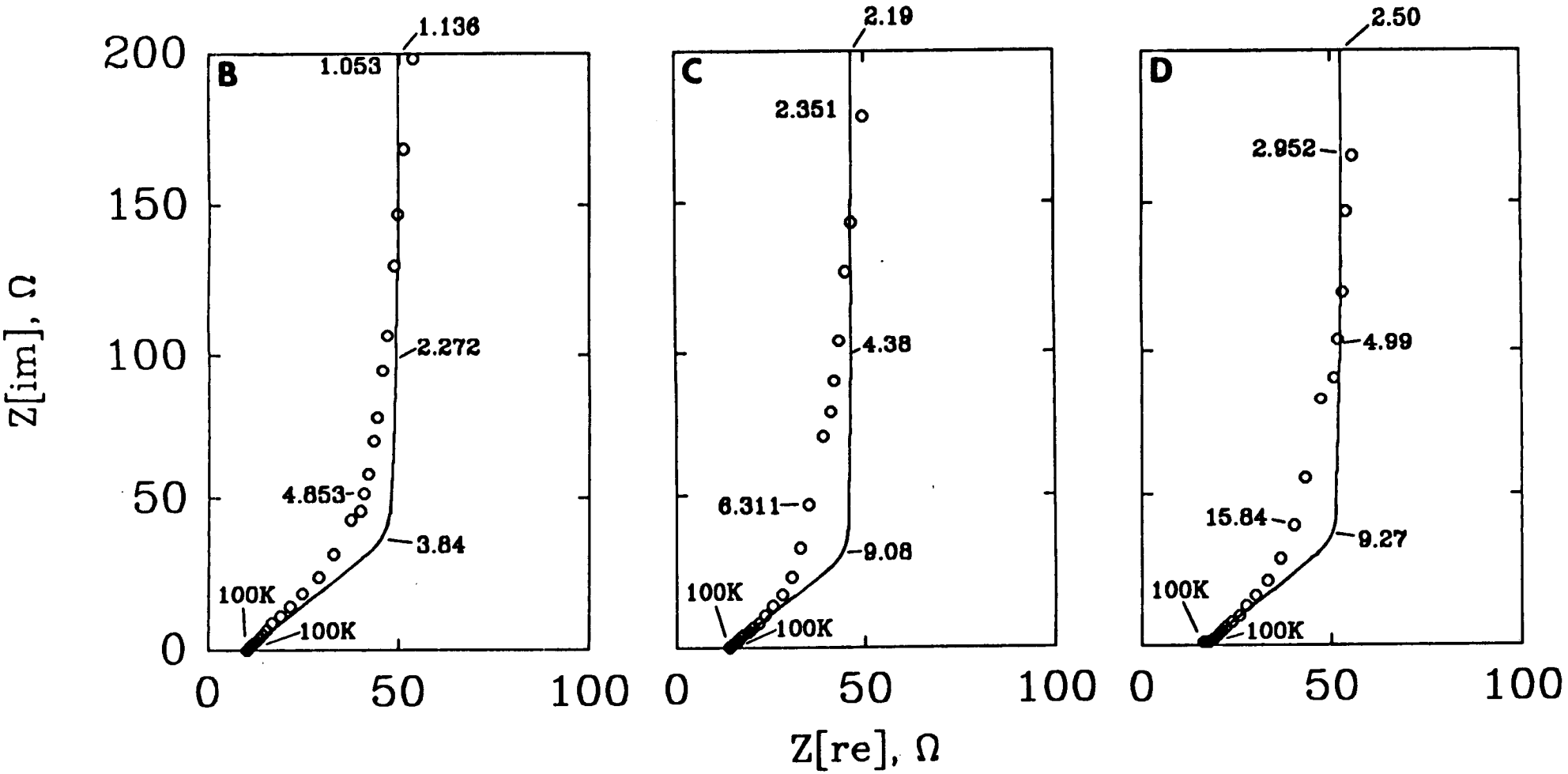
B
C
D
1.136
1.053
2.272
4.853
3.84
100K
100K
2.19
2.351
4.38
6.311
9.08
100K
100K
2.50
2.952
4.99
15.84
9.27
100K
100K
200
150
100
50
0
0
50
100
Z[im], Ω
Z[re], Ω

Figure 6-B,C,& D

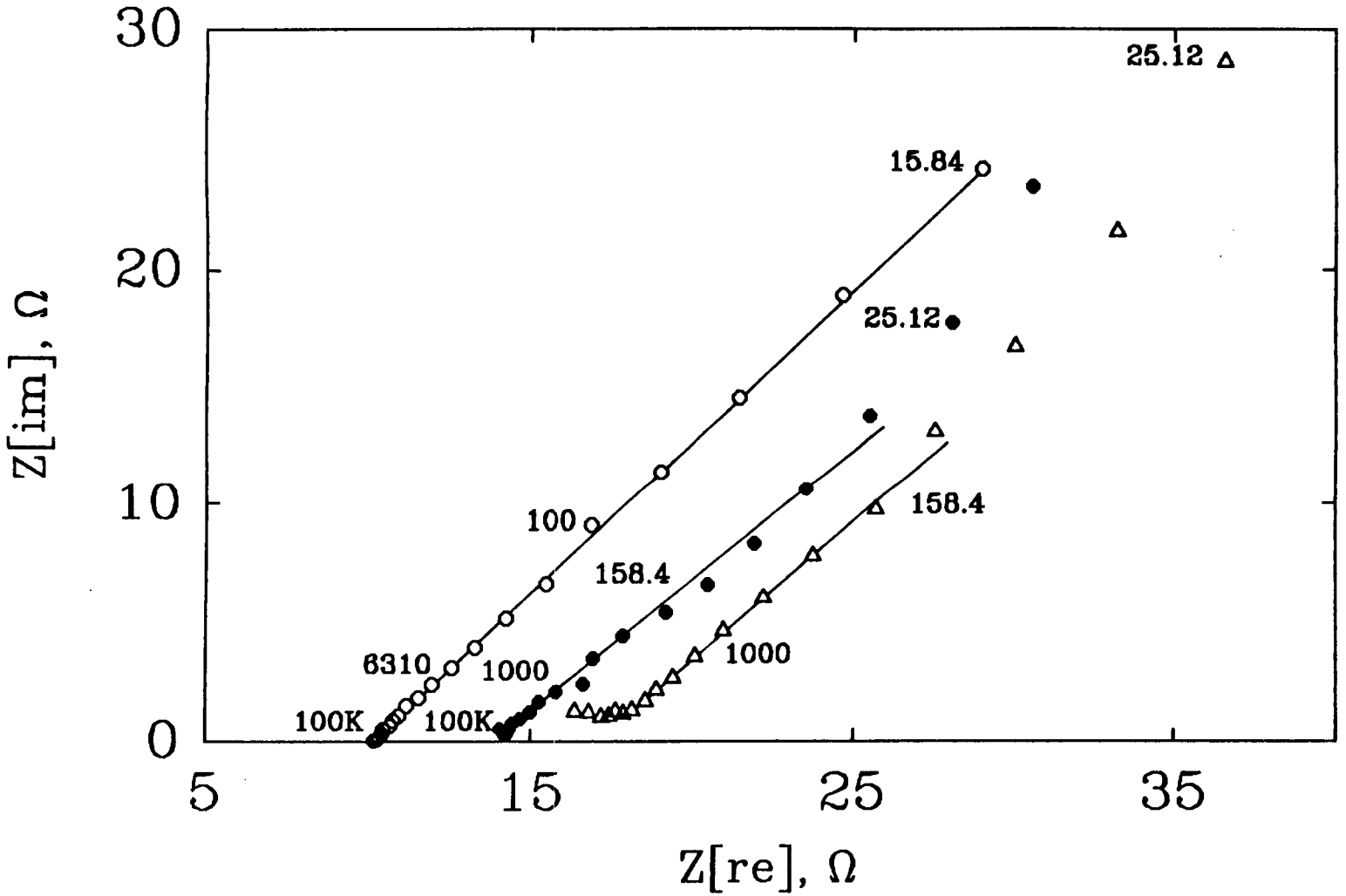
30
20
10
0
5
15
25
35
Z[im], Ω
Z[re], Ω
25.12
15.84
25.12
100
158.4
158.4
6310
1000
1000
100K
100K

Figure 7-A

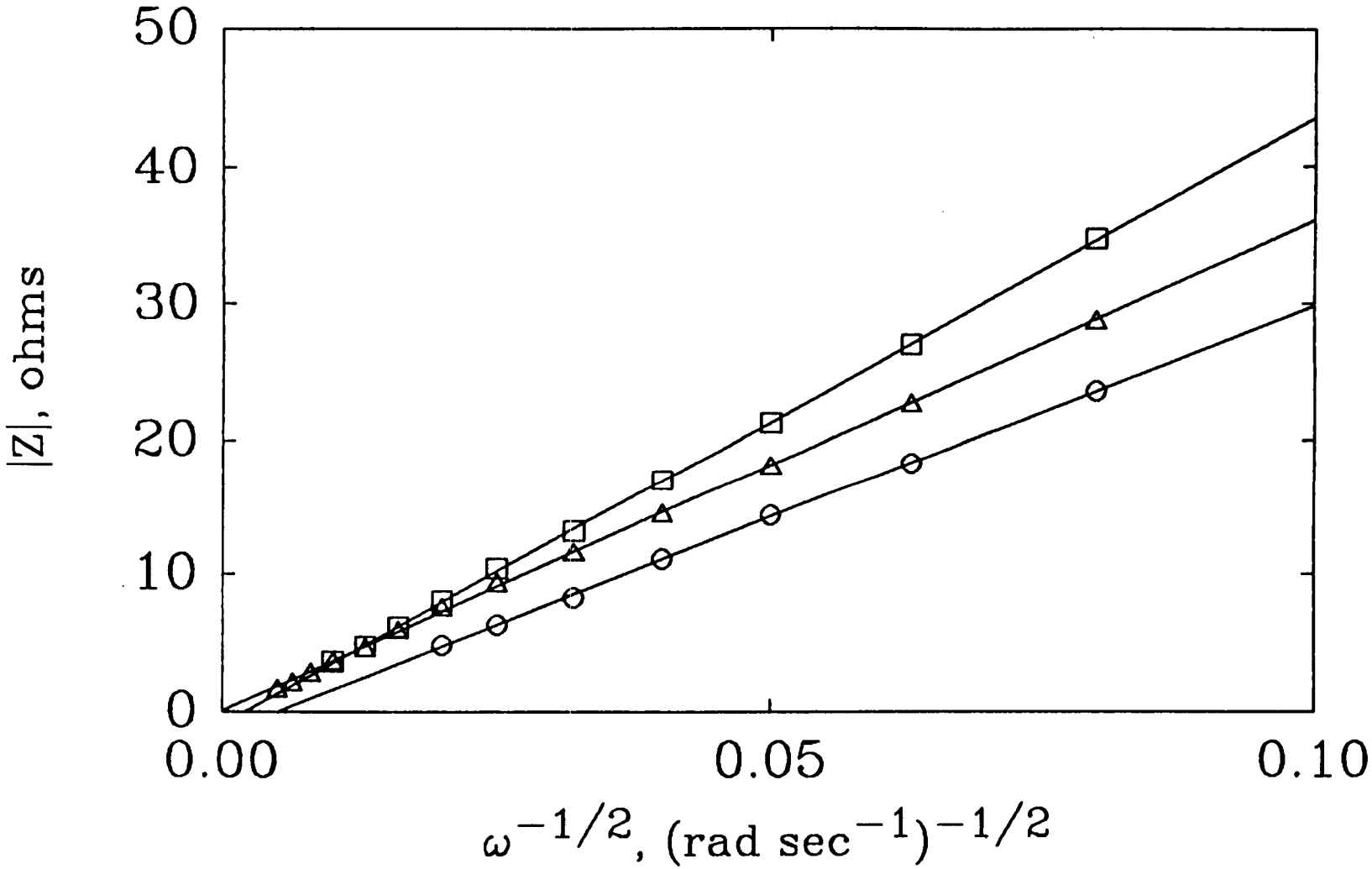


Figure 7-B

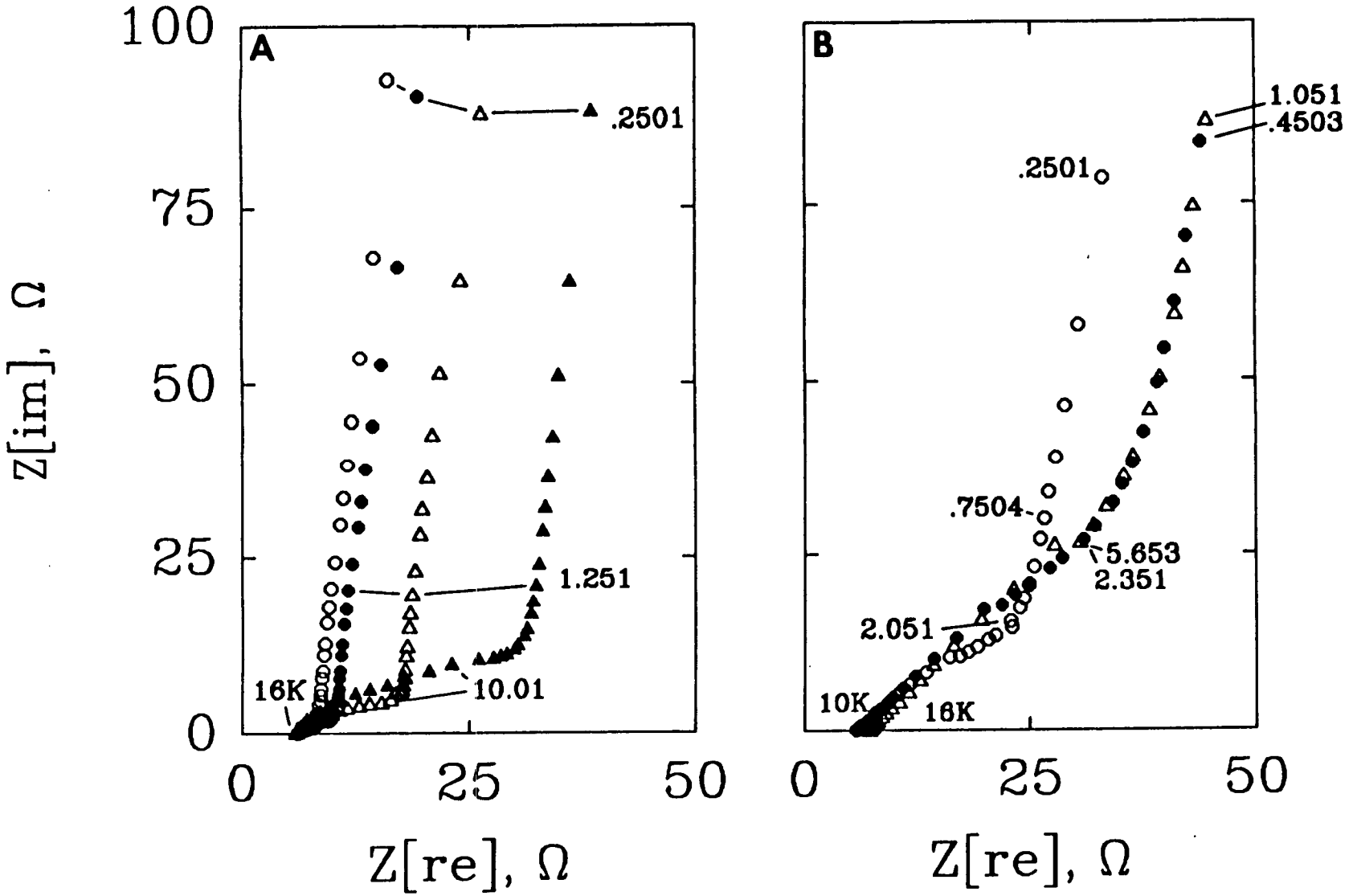
A
B
100
75
50
25
0
Z[im], Ω
.2501
1.251
10.01
16K
0
25
50
Z[re], Ω
1.051
.4503
.2501
.7504
5.653
2.351
2.051
10K
16K
0
25
50
Z[re], Ω

Figure 8-A,B

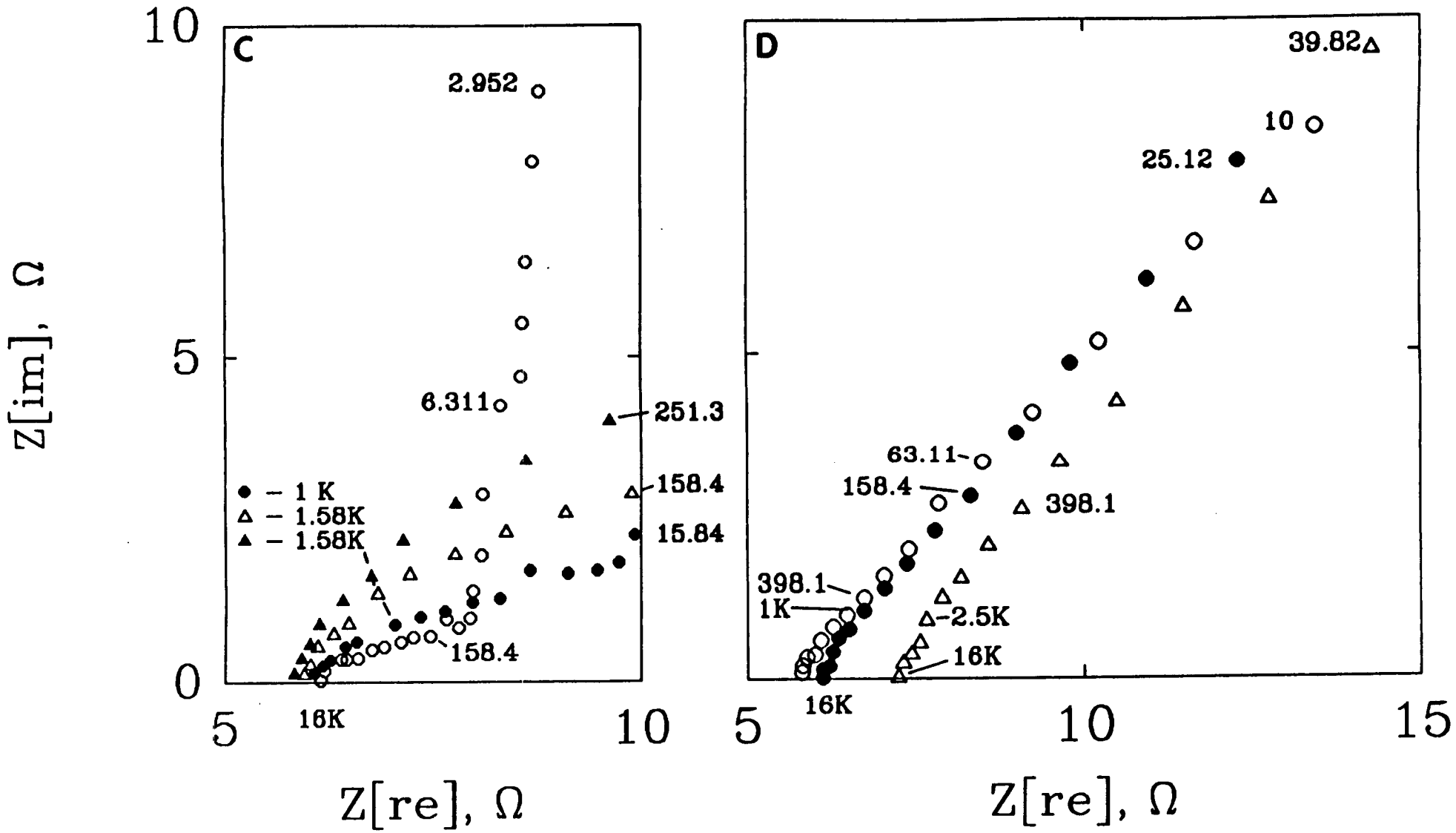
C
D
10
5
0
5
10
15
Z[im], Ω
Z[re], Ω
Z[re], Ω
2.952
6.311
251.3
158.4
15.84
158.4
16K
● – 1 K
△ – 1.58K
▲ – 1.58K
39.82△
10
25.12
63.11
158.4
398.1
398.1
1K
2.5K
16K
16K

Figure 8-C,D

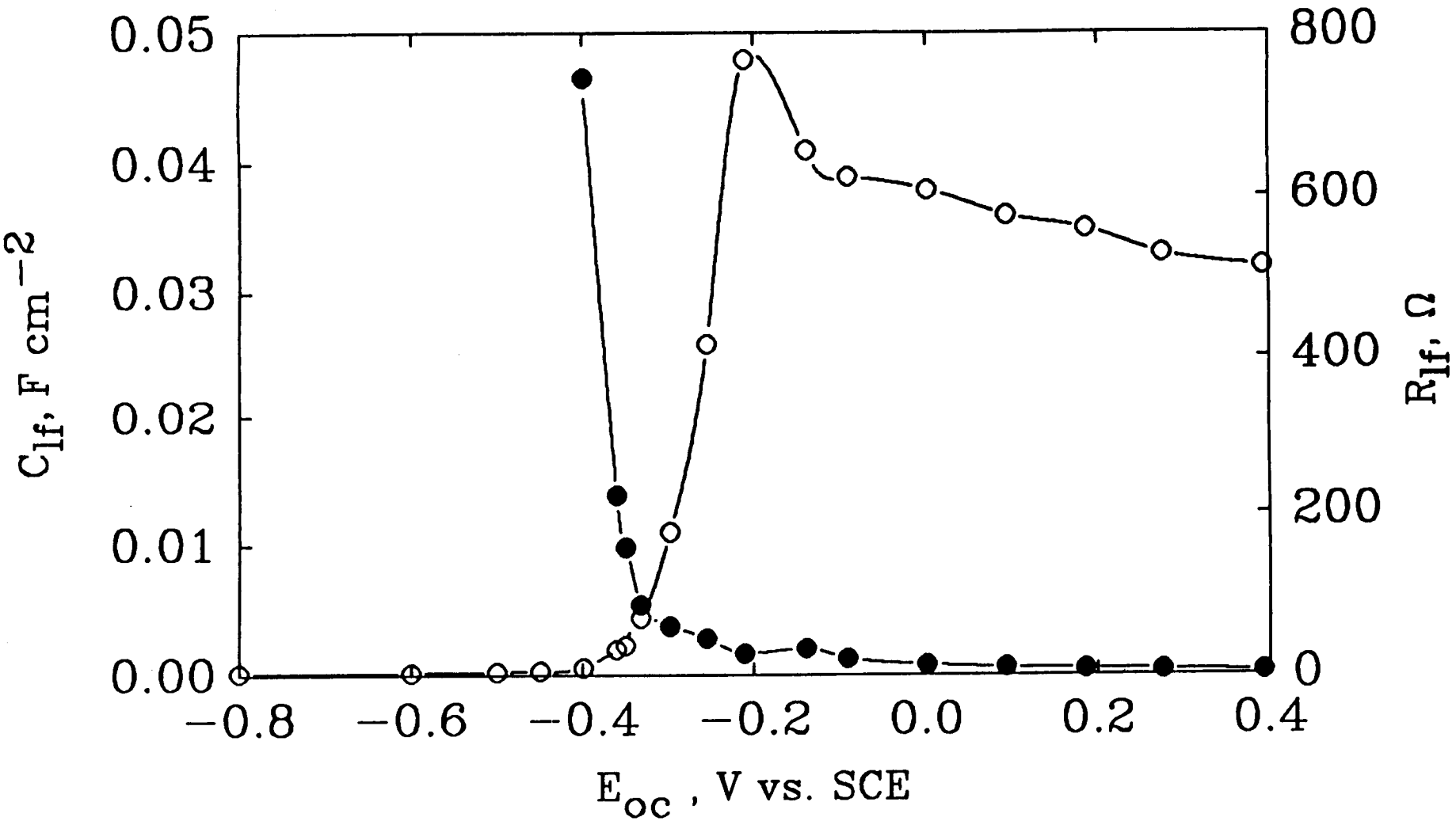
0.05
0.04
0.03
0.02
0.01
0.00
800
600
400
200
0
−0.8
−0.6
−0.4
−0.2
0.0
0.2
0.4
$C_{lf}$, F cm$^{-2}$
$R_{lf}$, Ω
$E_{oc}$ , V vs. SCE

Figure 9

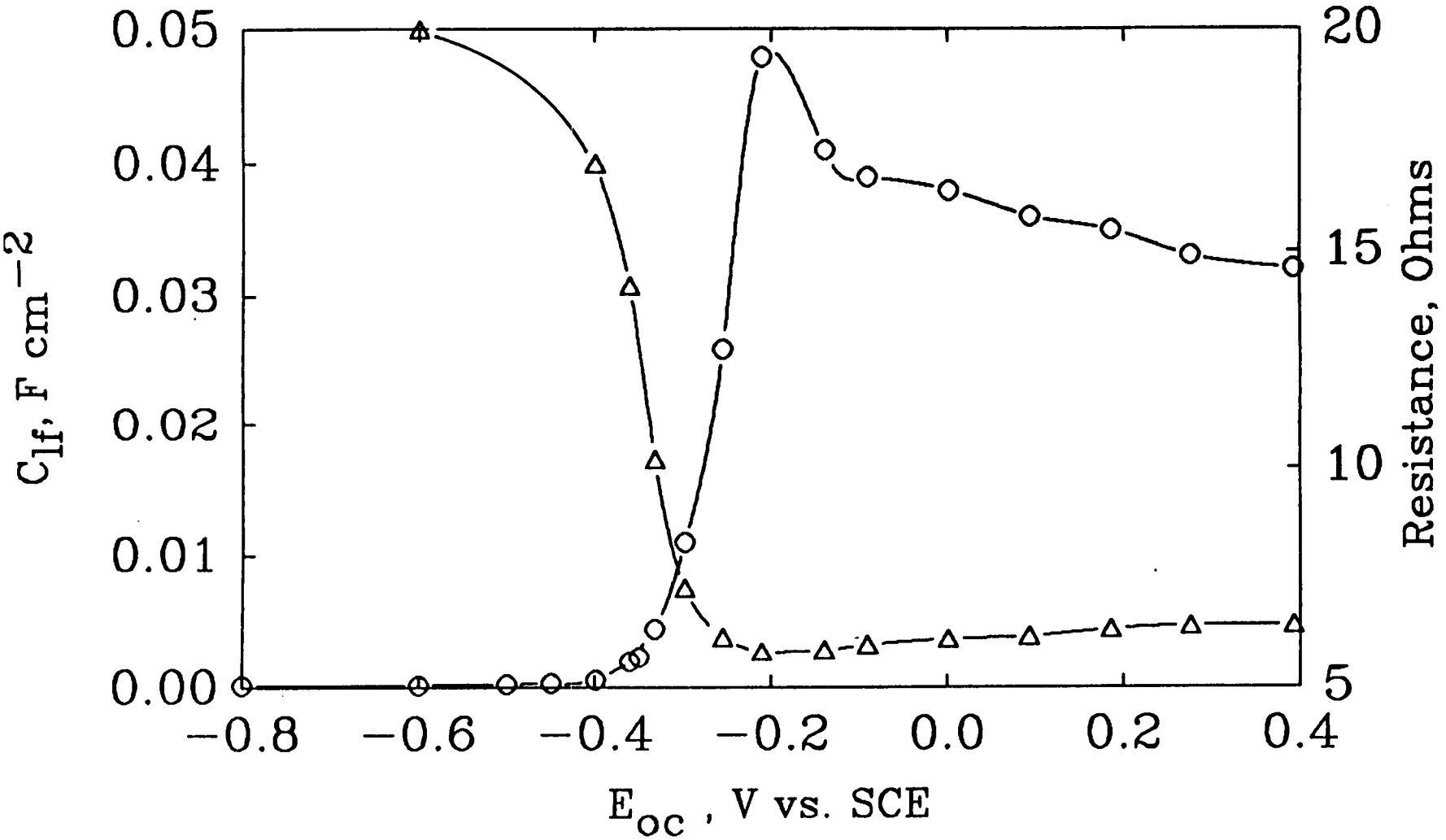
0.05
0.04
0.03
0.02
0.01
0.00
$C_{lf}$, F cm$^{-2}$
20
15
10
5
Resistance, Ohms
−0.8
−0.6
−0.4
−0.2
0.0
0.2
0.4
$E_{oc}$ , V vs. SCE

Figure 10